An Evaluation of Above- and In-Water Methods for Determining Water-Leaving Radiances

STANFORD B. HOOKER

NASA Goddard Space Flight Center, Greenbelt, Maryland

GORDANA LAZIN

Satlantic, Inc., Halifax, Nova Scotia, Canada

GIUSEPPE ZIBORDI

Joint Research Centre, Ispra, Italy

SCOTT MCLEAN

Satlantic, Inc., Halifax, Nova Scotia, Canada

(Manuscript received 30 August 2000, in final form 17 August 2001)

ABSTRACT

A high-quality dataset collected at an oceanographic tower was used to compare water-leaving radiances derived from simultaneous above- and in-water optical measurements. The former involved two different above-water systems and four different surface glint correction methods, while the latter used three different in-water sampling systems and three different methods (one system made measurements a fixed distance from the tower, 7.5 m; another at variable distances up to 29 m away; and the third was a buoy sited 50 m away). Instruments with a common calibration history were used, and to separate differences in methods from changes in instrument performance, the stability (at the 1% level) and intercalibration of the instruments (at the 2%–3% level) was performed in the field with a second generation Sea-viewing Wide Field-of-view Sensor (SeaWiFS) Quality Monitor (SQM-II). The water-leaving radiances estimated from the methods were compared to establish their performance during the field campaign, which included clear and overcast skies, Case-1 and Case-2 conditions, calm and roughened sea surface, etc. Three different analytical approaches, based on unbiased percent differences (UPDs) between the methods, were used to compare the various methods. The first used spectral averages across the 412–555-nm SeaWiFS bands (the part of the spectrum used for ocean color algorithms), the second used the ratio of the 490- and 555-nm bands, and the third used the individual (discrete) wavelengths. There were eight primary conclusions of the comparisons, which were considered within the context of the SeaWiFS 5% radiometric objectives. 1) The 5% radiometric objective was achieved for some in-water methods in Case-1 waters for all analytical approaches. 2) The 5% radiometric objective was achieved for some above-water methods in Case-2 waters for all analytical approaches, and achieved in both water types for band ratios and some discrete wavelengths. 3) The largest uncertainties were in the blue domain (412 and 443 nm). 4) A best-to-worst ranking of the in-water methods based on minimal comparison differences did not depend on the analytical approach, but a similar ranking of the above-water methods did. 5) Above- and in-water methods not specifically designed for Case-2 conditions were capable of results in keeping with those formulated for the Case-2 environment or in keeping with results achieved in Case-1 waters. 6) There was a significant difference between two above-water instruments oriented perpendicular with respect to the sun, but pointed in the same direction (best agreement) versus the opposite direction (worst agreement). 7) The overall intercomparison of all methods across Case-1 and Case-2 conditions was at the 9.1% level for the spectral averages, and at the 3.1% level for the band ratios (uncertainties other than those associated with implementing the individual methods account for 2%–4% and 1%–3% of these values, respectively). 8) A comparison with traditional regression analyses confirms the UPD conclusions.

1. Introduction and background

Spectral water-leaving radiance, $L_w(\lambda)$, is the central physical quantity for bio-optical studies in the upper ocean; whether determined from above- or in-water data, $\hat{L}_w(\lambda)$ and $\tilde{L}_w(\lambda)$, respectively, it must be accurately measured. The Sea-viewing Wide Field-of-view Sensor (SeaWiFS) Project, for example, requires $L_w(\lambda)$ uncertainties within 5% (Hooker et al. 1993b). This was shown to be achievable for in-water measurements in Case-1 waters using primarily a single methodology

Corresponding author address: Dr. Stanford B. Hooker, NASA, GSFC, Greenbelt, MD 20771.
E-mail: stan@ardbeg.gsfc.nasa.gov

(Hooker and Maritorena 2000), but the uncertainty associated with multiple methods has not been well quantified. The SeaWiFS calibration and validation plan (Hooker and McClain 2000) has emphasized in-water field work because when the plan was conceived, the above-water protocols were not as mature as the in-water protocols (Mueller and Austin 1992). Although there has been steady progress in defining the proper metrology for above-water measurements, intracomparisons within a group of accepted techniques have not occurred. More importantly, intercomparisons between above- and in-water methods have also not been thoroughly investigated, although individual comparisons are available in the literature (e.g., Pinkerton et al. 1999; Toole et al. 2000).

The main difficulty with above-water measurements is associated with correcting the observations for the effect of surface waves that introduce significant fluctuations into the glint and reflected skylight components of the surface radiance field. The problem is made more difficult by the presence of clouds, which increase the fluctuations and associated uncertainties. At present, there are several methods for surface glint correction that were developed for different environmental conditions, that is, clear or cloudy sky, and Case-1 or Case-2 water: Austin (1974); Morel (1980); Carder and Steward (1985); Bukata et al. (1988); Mueller and Austin (1995); Lee et al. (1996); Lazin (1998); and the recurring revision of the so-called SeaWiFS Ocean Optics Protocols by Mueller et al. (2000). All of the methods recognize the importance of making surface measurements free of sun glint effects, so the differences in the methods are primarily due to how sky glint contamination is removed from the surface signal.

The SeaWiFS ocean optics protocols deserve some extra comments because they were published (Mueller and Austin 1992) to publicly establish the measurement strategies to verify the SeaWiFS uncertainty goals of 5% in water-leaving radiances and 35% in chlorophyll *a* concentration (Hooker et al. 1992). From the very beginning, the protocols were considered an evolving prescription that would allow the research community to approach the unprecedented measurement uncertainties implied by the SeaWiFS goals (Hooker and Esaias 1993); research and development activities were acknowledged to be important elements for improving the state of the art in specific areas. It was always the intent of the SeaWiFS Project and the SeaWiFS Working Groups (Hooker et al. 1993a) that the ocean optics protocols would be periodically evaluated and revised to reflect technical advances during the SeaWiFS Project cycle (Mueller and Austin 1995).

Although the ocean optics protocols document agreed upon methods for making and analyzing optical measurements, they do not attempt to quantitatively resolve differences in accepted or newly emerging methods. Consequently, multiple techniques are discussed in the protocols for different types of measurements or platforms, but an unequivocal recommendation as to which is the most suitable over a wide range of conditions is not made—this type of quantitative experimentation is left to the individual investigator, which is one objective of this study.

The techniques considered here are as follows: Morel (1980); Carder and Steward (1985), and as further explained in Lee et al. (1996); the Mueller and Austin (1995) SeaWiFS protocol; and Lazin (1998). Hereafter, these methods are referred to as M80, C85, S95, and L98, respectively. Some clarification of the S95 method is needed because in its subsequent revision, there are three proposed, generalized classes of measurement methods, categorized by Mueller et al. (2000) as (a) calibrated radiance and irradiance measurements, (b) uncalibrated radiance and reflectance plaque measurements, and (c) calibrated surface polarized radiance measurements with modeled irradiance and sky radiance. The first method is associated with S95, the second with C85, and the third is not considered here.

The in-water techniques currently in use (Mueller 2000) are based primarily on the Smith and Baker (1984) method, hereafter referred to as S84. Variations are derived from the acquisition procedures (and platforms), and how the data are propagated to the surface. Two alternative techniques were implemented in the ProSoft[1] software for processing data collected with Satlantic, Inc. (Halifax, Canada) sensors. The ProSoft methods rely on a surface buoy to make measurements close to the sea surface and are categorized according to when the processing options were implemented, which occurred in 1994 and 1997, so the two are referred to hereafter as P94 and P97, respectively.

The Normalized Remote Sensing Reflectance (NRSR) Workshop (11–12 December 1997) established a baseline uncertainty in NRSR determined from in-water radiance profiles, combined with above-water measurements of solar irradiance, of approximately 5% for wavelengths less than 600 nm and a diffuse attenuation coefficient at 490 nm, $K(490)$, less than 0.1 m^{-1} (Hooker et al. 1999). The uncertainty estimate was based on results from the first SeaWiFS Data Analysis Round-Robin activity (Siegel et al. 1995), plus the third and fourth SeaWiFS Intercalibration Round-Robin Experiments (Mueller et al. 1996; Johnson et al. 1996, respectively).

Radiative transfer simulations of remote sensing reflectance measurements above a wave-roughened surface from Mobley (1999) showed the increase with wind speed (and resulting surface wave slope) of sky radiance and sun glint reflectance in total radiance viewed at the sea surface, relative to radiance from beneath the sur-

[1] ProSoft is a bio-optical data analysis and visualization program freely available from the Department of Oceanography at Dalhousie University (Halifax, Canada); it is written using MatLab™ software from Mathworks, Inc. (Natick, Massachusetts), and is available from raptor.ocean.dal.ca.

face. At wind speeds approaching 10 m s^{-1}, the superior nadir viewing angle was 40°, rather than the 30° used by many of the participants (and the 20° given in the original publication of S95). At lower wind speeds and a 40° viewing angle, an effective (and spectrally constant) surface reflectance of $\rho' = 0.028$ was recommended. There was a consensus at the workshop that comparative analyses need to be done, but with the following restrictions: $\lambda < 600$ nm, $K(490) < 0.1$ m^{-1}, percent cloud cover less than 20%, wind speed less than 10 m s^{-1}, and solar zenith angle 30°–60°. Data outside these ranges may be considered but should be excluded from the simpler comparison methods.

A field campaign was organized from 5 to 17 July 1998, sequential days of the year (SDY) 186–198, to evaluate above- and in-water measurements for SeaWiFS validation. The *Acqua Alta* oceanographic tower (AAOT), located about 15 km east of the city of Venice (12.5083°E, 45.3139°N), was chosen as the deployment site. Although the primary reason for selecting the AAOT was the ongoing use of the tower for bio-optical measurements within the framework of the Coastal Atmosphere and Sea Time Series (CoASTS) activity at the Joint Research Centre (JRC), the other reasons were its stability (towers do not pitch and roll like ships), the summer climatology was favorable for conditions in keeping with the NRSR Workshop recommendations, and its proximity to a strong coastal front. The water around the tower can be Case-1 or Case-2 depending on whether the coastal front is pushed on- or offshore. The opportunity for sampling different water types within one field campaign was very appealing.

The deployment was called the first SeaWiFS Bio-Optical Algorithm Round-Robin (SeaBOARR-98) experiment because the long-term objective is to evaluate the effect of the different measurement protocols on bio-optical algorithms from a variety of field campaigns. This study details the first goals and results in that long-term analysis.

1) Use two above-water sampling systems and four surface glint correction methods (M80, C85, S95, and L98) to intracompare $\hat{L}_w(\lambda)$ estimates.
2) Use three in-water sampling and analysis methods (S84, P94, and P97) to intracompare $\tilde{L}_w(\lambda)$ estimates.
3) Use radiometers with a common calibration history to minimize intercalibration uncertainties.
4) Intercalibrate and monitor the stability of the sensors in the field with a second generation SeaWiFS Quality Monitor (SQM), the so-called SQM-II, to separate differences in methods from changes in performance.
5) Characterize the environmental conditions of the site during the field campaign, particularly the bio-optically active constituents, to establish a background environmental variability level.
6) Intercompare the water-leaving radiances estimated from the above- and in-water methods.
7) Use the comparison results to evaluate and rank the overall capabilities of the various methods.

The latter objective carries with it some sensitivity because individual investigators are associated with most of the techniques under consideration, but it is a practical necessity because (a) it is not possible to repeatedly deploy to the field with a wide diversity of equipment to satisfy all possible protocols, so solitary recommendations are needed; and (b) large calibration and validation databases like the SeaWiFS Bio-Optical Archive and Storage System (Hooker et al. 1994) require metrics by which contributed data can be categorized in terms of quality and suitability for use.

2. Measurement and analysis methods

A detailed description of the AAOT is presented in Zibordi et al. (1999), so only a brief overview is given here. The water depth immediately below the tower is about 17 m and the composition of the nearby seafloor is primarily sand and silt. The tower is composed of four levels supported by four large pillars. The first (lowest) tower level, about 4.5 m above the water, has an open grid deck and no facilities. The second level is approximately 7 m above the water and contains the water filtering and hydrography laboratory plus a special open grid platform, 3.5 m wide, which extends 6.5 m over the sea toward the southeast. The Wire-Stabilized Profiling Environmental Radiometer (WiSPER) package is deployed from this platform. The third deck contains the main laboratory, and the fourth (uppermost) deck, at about 13 m above the water, contains a wind generator, solar panels, a variety of meteorological instruments, communications antennae, plus water storage tanks.

For SeaBOARR-98, the total number of optical in situ systems deployed on the AAOT was increased beyond the in-water WiSPER system to include the following above- and in-water instruments:

1) the SeaWiFS Surface Acquisition System (SeaSAS),
2) the Dalhousie University SeaWiFS Aircraft Simulator (DalSAS),
3) the miniature NASA Environmental Sampling System (miniNESS), and
4) the Dalhousie University Buoyant Optical Surface Sensor (DalBOSS).

The above-water systems were SeaSAS (SS) and DalSAS (DS); the in-water systems were miniNESS (MN), DalBOSS (DB), and WiSPER (WP). In addition, an SQM-II was set up in the water filtering and hydrography laboratory. The SQM-II, plus all the above- and in-water radiometers, were manufactured by Satlantic, Inc., and had very similar wavelengths and bandwidths. This commonality in equipment was the easiest

way to ensure redundancy and intercalibration, and it greatly simplified calibration monitoring with the SQM-II because all the radiometers had identical outer dimensions. Detailed descriptions of the radiometric systems are given in Hooker et al. (1999), so only a brief overview is given in Table 1.

a. Experimental setting and overview

Besides the in situ optical measurements, a variety of ancillary data are routinely collected at the AAOT to help characterize the bio-optical properties of the site during all field campaigns (presented and considered below). Although these ancillary measurements did not require augmentation, inclusion of additional radiometric systems for the SeaBOARR-98 deployment necessitated a more extensive mobilization phase prior to data collection. The basic data sampling activity involved collecting data from all of the instruments as simultaneously as possible, so handheld radios were used to coordinate the beginning and ending of sampling intervals.

The relative deployment locations of the instruments are shown in Fig. 1, along with the pointing nomenclature for the above-water systems, and a summary of all the instruments and what they measured is presented in Fig. 2. In addition to paying close attention to the optimal viewing capabilities of each instrument system, some instruments were equipped with sensors that measured their pointing angles. SeaSAS, for example, had an external module that measured the vertical (two-axis) tilts and horizontal (compass) pointing of the radiometers (the so-called DIR-10 unit); miniNESS and DalBOSS had internal sensors which measured the vertical (two-axis) tilts of the radiometers. All radiometric data were logged at full temporal resolution.

b. Radiometric stability and polarization sensitivity

Because this study deals with above- and in-water measurements, polarization effects can be a problem with the former. Polarization sensitivity within Satlantic above-water radiometers was recently determined to be about 0.9% (Hooker et al. 2002). Calibration stability is (potentially) a more important problem because previous deployments have shown significant and unpredictable differences in individual channels over the course of a field deployment (Hooker and Maritorena 2000). This problem was dealt with by monitoring the sensors in the field with a portable light source (an SQM-II).

The SQM is a compact light source developed for monitoring the radiometric stability of radiometers while they are being deployed in the field. Two computer-controlled power supplies and a multiplexed, digital voltmeter, are essential elements for producing the stable light field (Johnson et al. 1998). The SQM does not have, nor does it require, an absolute calibration, but it has design objectives and a demonstrated capability (Hooker and Aiken 1998) of approximately 1% stability during repeated field deployments (Hooker and Maritorena 2000). Two sets of halogen lamps with eight lamps in each set are arranged symmetrically on a ring. The lamps have different wattages, so a low, medium, and high intensity flux level is provided when the lamp sets are used individually and together.

Satlantic, Inc., developed the SQM-II as a commercial version of the SQM and based the design on the original (e.g., the same lamps were used). The main difference with the new unit is the high degree of integration in the control architecture, but several improvements, which experience with the original indicated were desirable, were made (McLean et al. 1998). The most notable difference is that the light chamber is lined with Spectralon, so the emitted flux and aperture uniformity are greater (at 490 nm, the SQM-II is about seven times more intense than the SQM). Although the greater flux of the SQM-II is a desireable attribute for the blue part of the spectrum, the high output in the red saturates many in-water radiometers. This was corrected by adding a blue filter to the exit aperture.

To monitor the stability (in the field) of the above- and in-water radiometers, and to quantify the performance of the SQM-II during its field commissioning, the procedures given in Hooker (2000) were followed where applicable. A calibration evaluation and radiometric testing session was defined, and a sequence of procedures was implemented for each one beginning with the SQM-II being warmed up until the internal SQM-II detector was constant to within 0.1%. After the warm-up period, each fiducial, or reflective standard, was measured, and then the individual radiometric sensors were tested sequentially. After all the radiometers were measured, the fiducials were measured again, the SQM-II was shut down, and the internal monitor dark voltages were recorded. The number of hours on each lamp set were tracked by recording the starting and ending number of hours on the lamp set. The fiducial data, acquired during radiometer dark measurements, were the primary sources for tracking the stability of the SQM-II flux.

c. In-water determinations of water-leaving radiances

The in-water experimental setup began with siting a marker buoy about 90 m from the southeast tower leg. A taught wire between the tower and the buoy anchor was used with a closed loop of line marked in 1-m intervals and strung between pulleys on the buoy and tower, to position miniNESS a selected distance from the tower (Hooker et al. 1999) or at 7.5 m (the distance at which WiSPER measurements were made). DalBOSS was secured to a second anchored buoy approximately 50 m from the tower. The sea and wave field was usually minimal, so there was little chance DalBOSS would pull against the marker buoy (which would accentuate the tilting of the sensor package), and there was no need to

TABLE 1. Sampling characteristics and center wavelengths (nm) for the radiometric sampling systems organized by their primary physical measurement, in terms of their vertical sampling, and their system (two-letter) codes. The former include the full-angle field of view (FOV), the sampling rate, the number of bits in the analog-to-digital (A/D) conversion, the amount of time to complete one sampling interval (typical duration), and the distance of the point of data collection from the tower, Δx (for the above-water systems this is a maximum distance computed from the height of the sensor above the water, the FOV of the sea-viewing sensor, and a perpendicular pointing with respect to the tower). SeaSAS, WiSPER, miniNESS, and DalSAS all used 7-channel ocean-color radiance series-200 (OCR-200) sensors and 7-channel ocean-color irradiance series-200 (OCI-200) sensors, which are both capable of detecting light over a four-decade range. DalBOSS was equipped with both 13-channel OCI and OCR series-1000 radiometers (OCI-1000 and OCR-1000, respectively), which use gain switching and are capable of detecting light over a 7-decade range. The bottom half of the table is organized by the sensor (letter-number) codes, which are formed from a one-letter designator for the type of sensor, plus a two-digit serial number. All of the channels had 10-nm bandwidths except the DalSAS sensors for which the 412-, 443-, 490-, 510-, and 555-nm channels had 20-nm bandwidths. Note that the M99 sensor was the solar irradiance reference for miniNESS, SeaSAS, and WiSPER, but it is only shown once for miniNESS. Wavelengths shown in bold face type indicate the primary channels used in the comparison analyses.

	MiniNESS (MN)			SeaSAS (SS)		WiSPER (WP)		DalSAS (DS)				DalBOSS (DB)	
Parameter	L_u (z)	E_d (z)	E_d (0$^+$)	L_i (0$^+$)	L_T (0$^+$)	L_u (z)	E_d (z)	L_i (0$^+$)	L_T (0$^+$)	E_d (0$^+$)	E_i (0$^+$)	L_u (z$_0$)	E_d (0$^+$)
FOV [°]	20	360	360	6	6	20	20	6	6	360	360	20	360
Rate [Hz]	6	6	6	6	6	6	6	10	10	10	10	6	6
A/D bits	16	16	16	16	16	16	16	16	16	16	16	24	24
Time [s]	20	20	20	180	180	360	360	180	180	180	180	180	180
Δx [m]	3–29	3–29	0	8.8	8.8	7.5	7.5	11.4	11.4	0	0	50	50
Sensor	R35	I40	M99	T69	T28	R46	I71	T64	T09	M20	M93	Q33	N48
Ch. 1	**411.1**	**411.5**	**411.5**	**412.6**	**412.7**	**412.3**	**411.3**	**412.7**	**412.7**	**412.6**	**412.5**	406.5	405.1
Ch. 2	**442.9**	**442.5**	**442.8**	**442.4**	**443.1**	**442.8**	**442.9**	**443.5**	**444.0**	**443.2**	**443.5**	**412.2**	**412.4**
Ch. 3	**489.9**	**489.3**	**489.9**	**491.3**	**489.5**	**490.5**	**490.2**	**490.0**	**491.5**	**491.5**	**490.0**	435.3	435.6
Ch. 4	**509.7**	**509.6**	**510.3**	**510.3**	**510.1**	**510.8**	**510.1**	781.9	780.7	781.6	781.7	**443.4**	**442.9**
Ch. 5	**554.8**	**555.4**	**554.5**	**554.1**	**554.8**	**554.9**	**554.8**	**510.9**	**510.5**	**509.8**	**509.3**	455.9	456.1
Ch. 6	665.0	665.7	664.8	669.8	670.0	665.8	665.6	**554.6**	**554.4**	**554.6**	**554.4**	**489.9**	**489.3**
Ch. 7	683.1	683.2	683.2	683.6	682.5	683.9	683.6	666.4	665.3	665.6	665.8	**510.4**	**510.4**
Ch. 8												531.6	531.5
Ch. 9												**554.6**	**554.5**
Ch. 10												590.3	590.4
Ch. 11												665.1	664.8
Ch. 12												670.0	670.0
Ch. 13												700.6	700.6

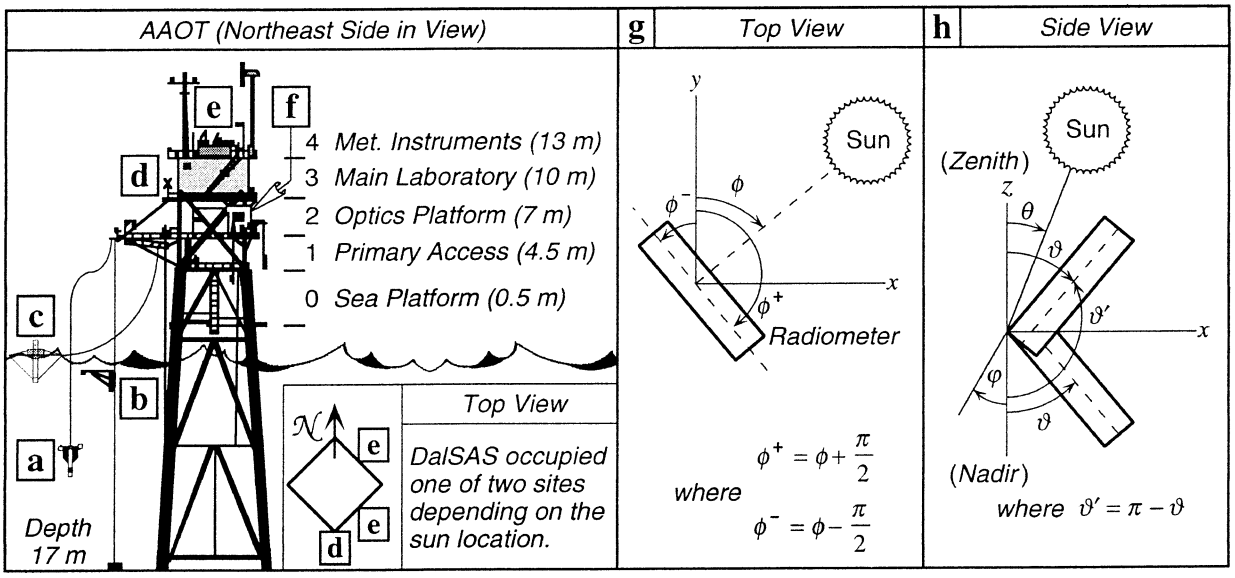

FIG. 1. The relative deployment locations of the various optical systems on the AAOT: (a) miniNESS, (b) WiSPER, (c) DalBOSS, (d) SeaSAS, (e) DalSAS, and (f) SQM-II. The coordinate systems used for pointing the above-water instruments are shown (g) looking down from above (the z axis is out of the page) and (h) looking from the side (the y axis is out of the page). The ϕ coordinate is the solar azimuth angle, θ is the solar zenith angle, and ϑ is the radiometer pointing angle with respect to the vertical axis, z. The perturbations (or tilts) in vertical alignment, which can change the pointing angles, are given by φ. Note that ϕ is measured with respect to an arbitrary reference, in this case due north, and ϑ is measured with respect to nadir (the direction pointing straight down to the sea surface). The angle ϑ' corresponds to the angle ϑ measured with respect to the zenith (the direction pointing straight up from the sea surface).

push the flotation collar down to elevate the irradiance sensor farther above the sea surface.

A miniNESS experiment was defined as a sequence of profile deployments going away or toward the platform during a short time period (typically 20 min), or as a series of casts at a fixed 7.5 m from the tower. The miniNESS profiler fell (mostly) freely through the water column (some tension was maintained on the line to prevent it from overshooting the termination point, defined by a cable block, and impacting the bottom). While the miniNESS casts were being sequentially collected, the WiSPER system was repeatedly lowered and raised in a series of triple casts.

1) MEASUREMENT METHODS

The miniNESS profiler measured upwelled radiance and downward irradiance as a function of depth, $L_u(z, \lambda)$ and $E_d(z, \lambda)$, respectively. A separate sensor measured the total solar irradiance (the direct plus the indirect or diffuse components) just above the sea surface $E_d(0^+, \lambda)$. Internal tilt sensors quantified the vertical orientation (φ) of the profiler as it fell through the water. The WiSPER package made the same measurements as miniNESS, $L_u(z, \lambda)$, and $E_d(z, \lambda)$, but it was slowly winched up and down the water column between two taught wires so it had no need for tilt sensors. In addition, the $E_d(z, \lambda)$ sensor was periodically rotated 180° to measure upwelling irradiance $E_u(z, \lambda)$. This special cast was executed in between two normal casts to measure $L_u(z, \lambda)$ and $E_d(z, \lambda)$.

DalBOSS is a variant of the SeaWiFS Buoyant Optical Surface Sensor (SeaBOSS), which was first deployed on the fifth Atlantic Meridional Transect cruise (Aiken et al. 1998). The radiometric sensor package was fitted inside a removable buoyant collar, secured within a floating square frame with elastic cords. The elastic cords absorb some of the energy of the ambient wave field and reduce sensor tilts (Hooker and Maritorena 2000). An irradiance sensor protruded up above the flotation collar to measure $E_d(0^+, \lambda)$ and a downward-looking radiance sensor at the bottom of the buoy measured the upwelled radiance at a depth (z_0) close to the sea surface, $L_u(z_0, \lambda)$. The advantage of this system was it could make measurements well clear of any perturbative effects associated with the superstructure of the tower (extra care was taken to keep the irradiance sensor dry during each deployment session).

2) DATA ANALYSIS METHODS

The ultimate purpose of the in-water approach is to extrapolate subsurface properties up to, and then through, the sea surface. Vertical sampling close to the air–sea interface ensures the needed amount of data to establish confidence in the extrapolation process. This approach is applicable to situations wherein the light sensors are fitted to mechanical supports at different depths (as is often the case with some buoys), but if the number of depths is reduced to one, the method fails. Alternative vertical sampling (P94) or modeling of the environment based on another property, like chlorophyll

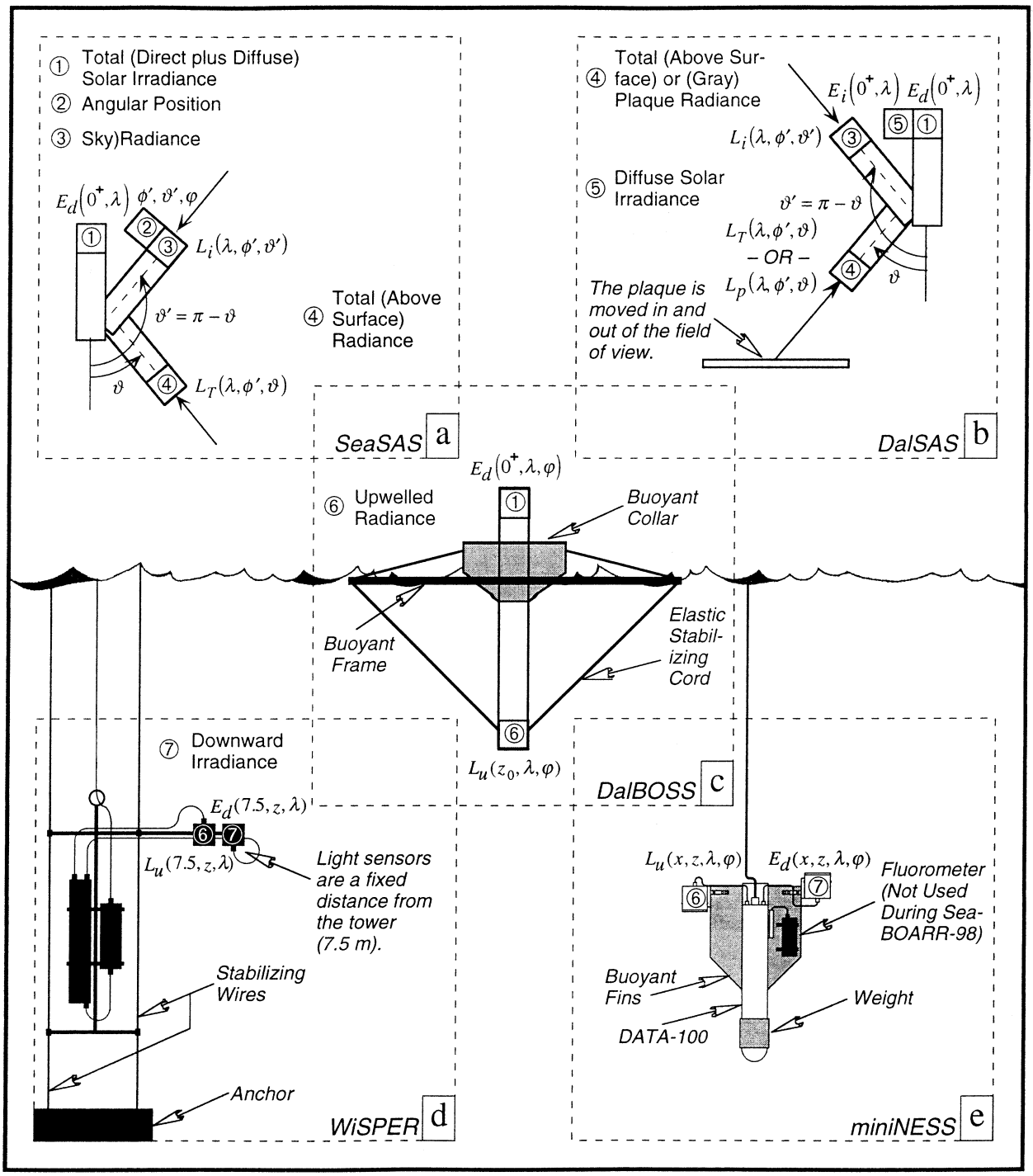

FIG. 2. A generalized schematic of the above- and in-water instruments used during SeaBOARR-98: (a) SeaSAS, (b) DalSAS, (c) DalBOSS, (d) WiSPER, and (e) miniNESS.

a concentration (P97), can be used to provide the information needed for extrapolation. For Case-1 conditions, using a single alternative variable to establish the bio-optical properties of the environment was shown to be acceptable (Morel 1988), but this is not expected to be true for Case-2 waters.

The processing of the data does not end with the calculation of water-leaving radiances. Because the

measurements are being made in the proximity of a large structure in shallow water, there are other considerations: instrument self-shading, bottom reflection, and tower shading. The latter affects all of the data except those from systems deployed more than 15 m away from the tower (DalBOSS and half of the miniNESS data). To maximize comparability, comparisons between WiSPER and miniNESS were done using only the miniNESS casts at 7.5 m from the tower when both data were similarly degraded by tower perturbations.

All of the in-water instruments have identical outer diameters, so an instrument self-shading correction was calculated for the WiSPER radiometers (Table 1) and applied to all of the in-water instruments (Zibordi and Ferrari 1995). A correction term for bottom reflection was usually calculated for the in-water data collected at the AAOT site, but no such correction scheme existed for the above-water data.

(i) Profiling Systems (S84)

The primary purpose of the S84 method is to estimate $\tilde{L}_W(\lambda)$ from a vertical profile of the water column. Although this is substantially different from the fixed-depth measurements associated with the other two in-water methods (P94 and P97), the underlying philosophy is common to all three, so it is presented in the most detail.

1) Bin the profiler data (if necessary), and compute the diffuse attenuation coefficient for upwelling radiance, $K_{L_u}(z_0, \lambda)$, from profiles of $L_u(z, \lambda)$ as the local slope of $\ln[L_u(z, \lambda)]$ in a depth interval of a few meters centered on depth z_0:

$$\ln[L_u(z, \lambda)] = \ln[L_u(z_0, \lambda)] - K_{L_u}(z_0, \lambda)\delta z, \quad (1)$$

where $\delta z = z - z_0$. The unknowns, $\ln[L_u(z_0, \lambda)]$ and $K_{L_u}(z_0, \lambda)$, are determined as the intercept and slope of a least-squares linear regression to the measured $\ln [L_u(z, \lambda)]$ data within the $z_0 - \Delta z \le z < z_0 + \Delta z$ interval. The Δz interval is somewhat arbitrary, but Smith and Baker (1984 and 1986) suggested a range of 4–10 m.

2) Extrapolate $L_u(z_0, \lambda)$ to the surface according to

$$L_u(0^-, \lambda) = L_u(z_0, \lambda) \exp[z_0 K_{L_u}(z_0, \lambda)]. \quad (2)$$

3) Transmit $L_u(0^-, \lambda)$ through the sea surface according to Austin (1974):

$$\tilde{L}_W(\lambda) = \frac{1 - \rho(\lambda, \vartheta)}{n_w^2(\lambda)} L_u(0^-, \lambda), \quad (3)$$

where $\rho(\lambda, \vartheta)$ is the Fresnel reflectance coefficient (at viewing angle ϑ, which for the in-water instruments is 0°), and $n_w(\lambda)$ is the refractive index of seawater. Austin (1980) noted the $[1 - \rho(\lambda, \vartheta)]n_w^{-2}(\lambda)$ expression can be replaced by a constant, because the wavelength dependence of the variables is very weak. The coefficient 0.54 has been shown to be the most appropriate for transmitting the normal radiance from below to above the sea surface regardless of the sea state (Mobley 1999). This substitution is made for all the in-water methods.

(ii) Fixed-depth systems (P94 and P97)

In the P94 method, the subsurface upwelling radiance measured at $z = 70$ cm is propagated to the sea surface using $K_{L_u}(\lambda)$ estimated from simultaneous $L_u(z, \lambda)$ profiles (following the techniques in S84) and then across the sea surface to produce $\tilde{L}_W(\lambda)$. The subsurface data were provided by DalBOSS, which had no profiling capability, so the $K_{L_u}(\lambda)$ data were provided by miniNESS because it was the most frequently deployed profiler.

In the P97 method, $L_u(443)/L_u(550)$ is used to estimate $K_{L_u}(490)$ and $K_{L_u}(520)$ as described by Austin and Petzold (1981). The computed $K_{L_u}(490)$ and $K_{L_u}(520)$ values are used to compute the chlorophyll *a* concentration, C_a, by inverting the algorithm for $K_{L_u}(\lambda)$ as detailed by Morel (1988). Once C_a is computed, $K_{L_u}(\lambda)$ for the other wavelengths can be computed using the Morel (1988) model. The subsurface upwelling radiance at $z = 70$ cm is propagated to the sea surface using the estimated $K_{L_u}(\lambda)$, and then across the sea surface to produce $\tilde{L}_W(\lambda)$.

d. Above-water determinations of water-leaving radiances

DalSAS was mounted 13.5 m above the water on the top-most deck, which had a number of superstructure obstacles. To ensure unperturbed viewing of the sea surface during as much of the day as possible, two sites were chosen: one on the northeast side and one on the southeast side. Depending on the time of day, DalSAS was moved from one location to the other. The two DalSAS irradiance sensors were positioned on the southeast side, and diffuse solar irradiance data, $E_i(0^+, \lambda)$, were collected by periodically occulting the appropriate irradiance sensor with a *lollipop* (a black 9-cm disk mounted on a 1-m rod). SeaSAS was mounted one deck below DalSAS on the southern corner 10.5 m above the water. When DalSAS was on the northeast side of the tower, SeaSAS was necessarily pointed 90° away; when it was on the southeast side, the two instruments were usually pointed in the same direction. In either case, there were times when the two instruments were pointed in the same and opposite directions with respect to one another (but perpendicular to the sun).

1) MEASUREMENT METHODS

The SeaSAS instruments measured the sky radiance reaching the sea surface, $L_i(0^+, \lambda)$, and the total radiance

right above the sea surface, $L_T(0^+, \lambda)$. The latter is composed of three terms: the radiance leaving the sea surface from below (the so-called water-leaving radiance), the direct sunlight reflecting off the surface (the so-called sun glint), and the skylight reflecting off the surface (the so-called sky glint). A separate sensor measured $E_d(0^+, \lambda)$ which, in this case, was the same sensor used with miniNESS (the irradiance sensor data was sent to both acquisition systems). DalSAS made the same measurements as SeaSAS, $L_i(0^+, \lambda)$ and $L_T(0^+, \lambda)$, but the surface-viewing radiometer looked through a square aperture that was periodically blocked with a gray plaque, so it also measured the radiance of the plaque, $L_p(0^+, \lambda)$. Two separate sensors were used to measure $E_d(0^+, \lambda)$ and $E_i(0^+, \lambda)$.

The gray plaque used was a 25 cm (10 in.) gray Spectralon™ plaque manufactured and calibrated by Labsphere, Inc. (North Sutton, New Hampshire), with a nominal 10% reflectance (SRT-10-100). This reflectance value permitted the radiometers with (typical) above-water saturation values to view the plaque under sunny conditions without saturating (approximately 6 μW cm^{-2} nm^{-1} sr^{-1}). Unlike the 99% reflectance of pure (white) Spectralon plaques, which are usually used for radiometric calibration, gray plaques are much less lambertian, because of the added impurities of the black doping material. Variations in viewing and illumination geometries, as are naturally found in the field, are likely to add significant variance in this measurement.

A directional/directional (i.e., 0°/45°) plaque calibration, instead of the standard directional/hemispherical calibration was used for this campaign, because this was closer to the actual field geometry. Before calibration, the homogeneity of the plaque was checked at a minimum of four spots on the plaque surface. There were no variations greater than 2% between the spots, so the plaque was recalibrated without any additional resurfacing (i.e., sanding). Although Spectralon is very hydrophobic, it readily absorbs grease and oil, which are very difficult to remove and can cause significant variance in calibrations. Special precautions were taken to avoid touching the diffusive material. To avoid long exposure to marine aerosols, the plaque was kept in a padded, airtight enclosure when not in use and only exposed during the measurement sequences. It was always wrapped in acid-free paper during transport and storage before, during, and after the field campaign.

2) Data analysis methods

Based on the consensus reached at the NRSR workshop (and Mobley 1999), all of the above-water methods in the SeaBOARR-98 field campaign used a nadir and zenith viewing angle of $\vartheta = 40°$ (this revision was incorporated into the second version of the ocean optics protocols). Although S95 explicitly states some common sense procedures, all of the methods make use of them, so they are assumed to be a part of all above-water methods. In particular, foam and floating material must be avoided during measurements, and because of temporal variability due to waves, it is important to record a number of spectra within a period of a few seconds (e.g., 30 spectra within 15 s).

Sea surface radiance data collected at high frequency in stable (sea and sky) conditions are a superposition of three contributions: (a) the steady, background water-leaving radiance; (b) the (mostly) random, sharp sun glint outliers; and (c) the variations in the sky glint from the waves. Some above-water techniques try to deal with the negative effects of glint at the point of measurement (Fougnie et al. 1999), but most deal with it explicitly by filtering it out or removing it with a correction scheme. The M80, C85, and L98 glint correction methods require the existence of a spectral band in the near infrared part of the spectrum (λ_r) for which $L_W(\lambda_r) = 0$. For the open ocean (Case-1 with $C_a < 0.25$ mg m^{-3}), the assumption $L_W(670) = 0$ can be used (Gordon 1981); for all other Case-1 waters, the 765- and 865-nm wavelengths should be used (Gordon and Wang 1994). For Case-2 waters, the assumption $L_W(1012) = 0$ has been found to be appropriate even in waters heavily loaded with sediment (Bukata et al. 1995).

The first revision of the ocean optics protocols incorporated new methodologies in several areas, including expanded protocol descriptions for Case-2 waters (Mueller and Austin 1995). All of the methods are applied to all of the data collected, regardless of the water or algorithm type, because in many cases optical data are collected without a full bio-optical characterization of the acquisition site. The performance of the various methods across a wide range of conditions is needed, not only to understand the consequences of inadvertently using a method inappropriately, but also to make progress on what are the desirable or negative aspects of algorithms within the global ocean.

There is also the consideration that all the SeaSAS and DalSAS (as well as the WiSPER) data were contaminated by tower-shading and bottom-reflection effects, but only the in-water data are currently correctable (Zibordi et al. 1999). To keep the above- and in-water data comparable, tower-shading corrections were not applied to the WiSPER data, and neither the above- or in-water data were corrected for bottom reflection. This equalizes the comparisons between the above-water instruments and WiSPER, but it leaves a source of variance when comparing the P94 and P97 (DB) results with the above-water methods because they were not contaminated by tower perturbations.

(i) Near-infrared radiance ratio glint correction (M80)

In the M80 method, temporal sun glint from the high frequency spectra is removed before averaging, so the final mean spectrum incorporates sky glint only. The sky glint correction is based on the assumption that

water-leaving radiance in a near-infrared band, λ_r, is negligible. Consequently, the above-water radiance measured at λ_r is due entirely to surface reflection. The infrared estimate of sky glint is extended over the whole spectrum by using the measured wavelength dependence of the incident sky radiance. Estimated sky glint is subtracted from the total signal to recover $\hat{L}_W(\lambda)$:

$$\hat{L}_W(\lambda) = L_T(\lambda, \phi', \vartheta) - L_i(\lambda, \phi', \vartheta')\left[\frac{L_T(\lambda_r, \phi', \vartheta)}{L_i(\lambda_r, \phi', \vartheta')}\right], \quad (4)$$

where $\phi' = \phi \pm \pi/2$ (90° away from the sun in either direction, i.e., ϕ^+ or ϕ^- in Fig. 1).

(ii) Fresnel reflectance plus residual reflection correction (C85)

The C85 method uses data averaged over 10-s intervals, so each spectrum of sea surface radiance incorporates the contribution of temporal sun glint. The above-water measurements are corrected for sky glint assuming specular reflection of sky radiance at the sea surface. The residual reflection of downwelling radiation from the wave facets is computed assuming the residual signal in the near infrared domain is entirely due to surface reflection, that is, $L_W(\lambda_r) = 0$. This term is estimated with a horizontally oriented gray reflectance plaque with reflectance $\rho_p(\lambda, \vartheta)$:

$$\Delta L = [L_T(\lambda_r) - \rho(\lambda, \vartheta)L_i(\lambda_r, \phi', \vartheta')]\frac{E_p(\lambda)}{E_p(\lambda_r)}, \quad (5)$$

where $E_p(\lambda) = \pi L_p(\lambda, \phi', \vartheta)/\rho_p(\lambda, \vartheta)$. $\hat{L}_W(\lambda)$ is computed by accounting for both correction terms:

$$\hat{L}_W(\lambda) = L_T(\lambda, \phi', \vartheta) - \rho(\lambda, \vartheta)L_i(\lambda, \phi', \vartheta') - \Delta L. \quad (6)$$

Note the use of $\rho(\lambda, \vartheta)$ rather than ρ'—the C85 method specifically uses the Fresnel reflectance.

For the purposes of this study, C85 is considered a Case-2 algorithm. The use of C85 in Case-2 waters requires more explanation: this method was devised for Case-1 conditions (Lee et al. 1996), but the formulation of the algorithm (which closely matches S95) and the small size of the correction term (ΔL) suggests it should be suitable for Case-2 waters without a heavy sediment load (like the Adriatic Sea). In terms of the published criteria for its use (Lee et al. 1996), it can be used confidently, cautiously, or uncertainly depending on the $R_{rs}(440)/R_{rs}(550)$ ratio (greater than 1.0, between 1.0 and 0.5, and less than 0.5, respectively).

(iii) Modified fresnel reflectance glint correction (S95)

The S95 formulation is based on the version-1 revision of the ocean optics protocols, which requires the radiometer to be pointed at the sea surface at an angle $\vartheta = 20°$ (from nadir) and away from the solar azimuth angle (ϕ) by at least 90°, that is, ϕ'. Before calculating the final spectra, outliers are removed by computing mean (μ) and standard deviation (σ) estimates and rejecting spectral values more than 1.5 σ from the mean. $L_T(\lambda)$ is corrected for sky glint using measurements of $L_i(\lambda)$ in the direction appropriate for the specular reflection from the sea surface into the sensor. Here, $L_i(\lambda)$ measurements are made by pointing the radiometer into the sky at a zenith angle equal to the nadir angle of the $L_T(\lambda)$ observations (or as in Fig. 1, $\vartheta' = \pi - \vartheta$) and with the same azimuth angle.[2] The sky glint is removed using the surface reflectance:

$$\hat{L}_W(\lambda) = L_T(\lambda, \phi', \vartheta) - \rho(\lambda, \vartheta)L_i(\lambda, \phi', \vartheta'). \quad (7)$$

With respect to the version-1 formulation, note the replacement of $\rho(\lambda, \vartheta)$ with ρ', as per the recommendations of the NRSR Workshop, Mobley (1999), and the most recent version of the ocean optics protocols (Mueller et al. 2000), which also recommended nadir and zenith viewing angles of 40°. Also note the formulation in (7) is not the only above-water method discussed in the ocean optics protocols, and some investigators have interpreted the C85 method discussion in the protocols as the recommended method (e.g., Toole et al. 2000).

(iv) Near-infrared irradiance ratio glint correction (L98)

Sky glint correction for the L98 method is also based on the assumption that $\hat{L}_W(\lambda_r) = 0$, so the signal in the λ_r part of the spectrum is wholly attributable to surface reflection. The L98 method uses the wavelength dependence of diffuse sky irradiance to extend the estimate of sky glint at λ_r over the whole spectrum. The advantage of this method is that it incorporates the effect of clouds. The technical advantage is that $E_d(0^+, \lambda)$ and $E_i(0^+, \lambda)$ can be measured with the same instrument: an upward-viewing radiometer where the diffuse component can be determined by periodically blocking the direct solar illumination of the radiometer, so $E_d(0^+, \lambda)$ and $E_i(0^+, \lambda)$ can be continuously monitored during remote sensing observations. Estimated sky glint is subtracted from the total signal to recover $\hat{L}_W(\lambda)$:

$$\hat{L}_W(\lambda) = L_T(\lambda, \phi', \vartheta) - \left[\frac{L_T(\lambda_r)}{E_i(\lambda_r)}\right]E_i(\lambda). \quad (8)$$

[2] The original S95 protocol included the option of measuring $L_i(\lambda)$ by looking at a horizontal *first surface* mirror (a mirror with no layers other than the reflective surface) at the same nadir and azimuth angles used for the $L_T(\lambda)$ observations. This would strongly repolarize the sky radiance and produce a significant measurement artifact, so this practice was dropped from the version-2 revision of the ocean optics protocols (Mueller et al. 2000).

TABLE 2. A summary of the three in-water methods for calculating $\tilde{L}_w(\lambda)$. The assumptions for each method and the input measurements required by the method are given in the second and third columns, respectively; the algorithms for calculating the water-leaving radiances are shown in the fourth column. All the techniques can be used in Case-1 conditions, but only S84 and P94 can be used in Case-2 waters, so P97 is shown in bold face. The latter makes use of the Morel (1988) model to estimate $K_{L_u}(\lambda)$, and this model is only appropriate for the case-1 environment.

Method	Assumptions	Input variables	$\tilde{L}_w(\lambda)$ calculation
S84	$z_0 - \Delta z \le z < z_0 + \Delta z$ $\Delta z \approx 4$ to 10 m	$K_{L_u}(z, \lambda)$ from $L_u(z, \lambda)$ $L_u(0^-, \lambda) = L_u(z_0, \lambda) \exp[z_0 K_{L_u}(z_0, \lambda)]$	$\tilde{L}_w(\lambda) = 0.54\, L_u(0^-, \lambda)$
P94	$z_0 - \Delta z \le z < z_0 + \Delta z$ $\Delta z \approx 4$ to 10 m	$K_{L_u}(z, \lambda)$ from $L_u(z, \lambda)$ $L_u(0^-, \lambda) = L_u(0.7, \lambda) \exp[0.7\, K_{L_u}(\lambda)]$	$\tilde{L}_w(\lambda) = 0.54\, L_u(0^-, \lambda)$
P97	$K_{L_u}(490, 520)$ from $L_u(443, 550)$ and C_a from $K_{L_u}(490, 520)$	$\chi(\lambda)$ and $e(\lambda)$ using Morel (1988) $K_{L_u}(\lambda) = K_w(\lambda) + \chi(\lambda) C_a^{e(\lambda)}$ $L_u(0^-, \lambda) = L_u(0.7, \lambda) \exp[0.7\, K_{L_u}(\lambda)]$	$\tilde{L}_w(\lambda) = 0.54\, L_u(0^-, \lambda)$

e. Comparison and statistical methods

The comparisons of the methods are organized by splitting them into two groups, above-water and in-water, and then considering the differences within and between groups. This produces three comparison possibilities, the first of which are the intracomparisons of the three in-water methods summarized in Table 2. The intracomparisons of the four above-water methods, incorporating the recommendations from the NRSR Workshop as summarized in Table 3, are presented next. The intercomparisons of all the methods are presented last.

Based on the formulations of the algorithms, the P94 and P97 methods are similar to one another, as are the M80 and L98 methods, and the C85 and S95 methods. All the techniques can be used in Case-1 conditions; S84, P94, C85, and S95 are the only methods formulated for the Case-2 environment. Because either above- or in-water measurements yield estimates of $L_w(\lambda)$, and, for the purposes of this study, neither is assumed to be more correct than the other, an unbiased parameter is needed to compare the various methods.

1) UNBIASED PERCENT DIFFERENCES

The unbiased percent difference (UPD) between two data products X^A and X^B determined from simultaneous casts at time t was computed as

$$\psi_B^A(\lambda, t) = 200 \frac{|X_i^A(\lambda, t) - X_i^B(\lambda, t)|}{X_i^A(\lambda, t) + X_i^B(\lambda, t)}, \qquad (9)$$

where the A and B codes identify the methods used, and the factor 200 occurs because the denominator is the average and the quotient is expressed as a percent. Absolute differences are used to ensure cancellation in any averages do not artificially lower the differences in the comparisons. Average UPD values over a particular set of data (e.g., data collected during one day) were computed as

TABLE 3. A summary of the four surface glint correction methods applied to the above-water radiance measurements. The measurement angles are based on the original protocols and the NRSR Workshop, $\vartheta = 40°$, $\vartheta' = 140°$, and $\phi' = 90°$ [the current protocols (Mueller et al. 2000) recommend $\phi' = 135°$ as the preferred azimuth geometry, and also recommend the use of Mobley's ρ', rather than the Fresnel reflectance]. All of the methods require ideal sky conditions (cloud free or uniformly overcast), except L98, which can be used under a variable sky. For all of the SeaBOARR-98 data, $\lambda_r = 780$ nm. All of the methods can be used in the Case-1 environment, but only the S95 and C85 methods can be used in Case-2 conditions [see section 2d(2)ii for a discussion on the limitations of using the latter in Case-2 waters], so the M80 and L98 methods are shown in bold face.

Method	Assumptions	Input variables	$\hat{L}_w(\lambda)$ calculation
M80	$L_w(\lambda_r) = 0$ and ideal sky	$L_T(\lambda)$ and $L_i(\lambda)$	$\hat{L}_w(\lambda) = L_T(\lambda, \phi', \vartheta) - L_i(\lambda, \phi', \vartheta') \left[\frac{L_T(\lambda_r, \phi', \vartheta)}{L_i(\lambda_r, \phi', \vartheta')}\right]$
C85	$L_w(\lambda_r) = 0$ and ideal sky	$L_T(\lambda)$, $L_i(\lambda)$, and $L_p(\lambda)$	$\hat{L}_w(\lambda) = L_T(\lambda, \phi', \vartheta) - \rho(\lambda, \vartheta) L_i(\lambda, \phi', \vartheta') - \Delta L$ where $\Delta L = [L_T(\lambda_r) - \rho(\lambda, \vartheta) L_i(\lambda_r, \phi', \vartheta')] E_p(\lambda)/E_p(\lambda)_r)$ and $E_p(\lambda) = \pi L_p(\lambda, \phi', \vartheta)/\rho_p(\lambda, \vartheta)$
S95	ρ' and ideal sky*	$L_T(\lambda)$ and $L_i(\lambda)$	$\hat{L}_w(\lambda) = L_T(\lambda, \phi', \vartheta) - \rho' L_i(\lambda, \phi', \vartheta')$
L98	$L_w(\lambda_r) = 0$	$L_T(\lambda)$ and $E_i(\lambda)$	$\hat{L}_w(\lambda) = L_T(\lambda, \phi', \vartheta) - \left[\frac{L_T(\lambda_r)}{E_i(\lambda_r)}\right] E_i(\lambda)$

* The ocean optics protocols indicate S95 can "probably" be used under variable cloud conditions.

$$\overline{\psi}_B^A(\lambda) = \frac{1}{M}\sum_{i=1}^{M} \psi_B^A(\lambda, t_i), \quad (10)$$

where M is the number of measurements, that is, the average UPD between the water-leaving radiances estimated with the M80 and S84 methods is $\overline{\psi}_{S84}^{M80}(\lambda)$.

Spectral averages of the UPD were formed by summing and weighting (10) over the blue-green wavelengths used for ocean-color algorithms, that is, the first five spectral bands:

$$\Psi_B^A(\lambda_{1-5}) = \frac{1}{5}\sum_{j=1}^{5} \psi_B^A(\lambda_j). \quad (11)$$

When a particular method type was compared against another, the *All* nomenclature is used with an overline—for example, $\overline{\Psi}_{P94}^{All}$ is the overall spectrally averaged UPD computed in comparing all the indicated methods to the P94 method.

Although the primary interest is in spectral estimates of water-leaving radiance, the most frequently used ocean color algorithms use band ratios (e.g., the OC2 algorithm uses the ratio between the 490- and 555-nm bands; O'Reilly et al. 1998). Consequently, another important parameter is the UPD between band ratios of water-leaving radiances:

$$\Phi_B^A(\lambda_{k/l}) = \frac{200}{M}\sum_{i=1}^{M} \frac{|L_W^A(\lambda_{k/l}, t_i) - L_W^B(\lambda_{k/l}, t_i)|}{L_W^A(\lambda_{k/l}, t_i) + L_W^B(\lambda_{k/l}, t_i)}, \quad (12)$$

where $L_W(\lambda_{k/l}, t)$ is the $L_W(\lambda_k, t)/L_W(\lambda_l, t)$ ratio, and the k and l indices set the channel numbers being used; that is, the average UPD value for the 490- and 555-nm band ratio is $\Phi_B^A(\lambda_{3/5})$. In most cases, the methods involved are explicitly stated, so the $\Phi_{3/5}$ shorthand notation is frequently used [the same is true for $\Psi_B^A(\lambda_{1-5})$ for which the abbreviated notation is Ψ_{1-5}].

2) Comparison strategies and metrics

The comparison strategies used in this study are a reflection of the large diversity in methods and instrumentation, as well as the complexity of the near-coastal environment. The primary requirement is to ensure the comparisons reflect only the differences in the methods, and not differences arising from external factors that might change from one method or instrument to another. Consequently, the first strategy is to use the smallest number of instruments possible to implement all the methods. To then provide a common basis for the evaluation of the methods, the second strategy is to estimate, and remove where possible, any extraneous sources of variance. The latter includes environmental variability, sensor stability and intercalibration, and the use of a single glint filter method in the above-water methods. The third strategy is to only use UPD statistics as the comparison metric, because they are unbiased, and to evaluate the results in terms of the stated radiometric objectives (i.e., the minimum acceptable uncertainty is to within 5%, and the desired uncertainty is to within 3%).

The final strategy is to separate the results according to water type, Case-1 or Case-2, and to present the results using a three-step process encompassing a broad-to-focused perspective. Spectral averages in the 412–555-nm domain are used to synthesize an overview from which the details are discerned using a band-ratio analysis followed by a discrete wavelength investigation. The latter uses the best above- and in-water methods identified by the other two analyses. The advantage of this scheme is it partitions an otherwise large and complex matrix of possible products into well-defined and manageable subsets.

The band-ratio analysis is restricted to the 490- and 555-nm band ratio in water-leaving radiance. There are three reasons for considering such an option: (a) one of the dominant ocean-color algorithms, OC2, uses the 490- and 555-nm band ratio as its primary input variable; (b) differences in applied corrections (e.g., tower shading) are somewhat mitigated by the band-ratio process; and (c) spectral deviations might be persistently biased, that is, parts of the spectrum might be shifted in the same direction and magnitude, so a ratio analysis might not be as unsatisfactory as a spectral analysis. The latter is particularly relevant to the above-water methods because glint contamination elevates broad sections of the spectrum.

The spectral aspects of glint makes it important to use the same glint filter with the above-water methods if possible. The M80, S95, and L98 methods require the removal of temporal sun glint (plus anomalous values due to foam and floating material) from the high frequency $L_T(\lambda)$ spectra, whereas C85 uses 10-s data averaging as part of the acquisition event, so glint contributions are convolved with the water-leaving radiance. Of the methods using glint filtering, only S95 includes a prescribed filter as part of the method. In order to study the effect of filtering in estimating $\hat{L}_W(\lambda)$, seven different filters are considered later in Table 5. The F_1 filter is the original S95 filter, F_2 is the revised S95 filter (Hooker and Lazin 2000), and the amount of filtering increases with increasing filter number (i.e., the amount of data retained decreases with increasing filter number).

3. Extraneous sources of variance

Hooker and Maritorena (2000) considered the total uncertainty arising from in-water optical data collection in the Case-1 environment as a function of a variety of deployment systems. They considered four sources of uncertainty: (a) calibration, (b) in situ sensor stability, (c) data collection method, and (d) data processing. A potential fifth uncertainty from environmental variability was assumed negligible, because all the data were collected from simultaneous casts in primarily homogeneous waters of the deep ocean. Furthermore, the data

processing uncertainty was not fully expressed, because only one data processor was used, and was restricted to how the uncertainty associated with extrapolations of $L_u(z, \lambda)$ to the surface, affect the comparisons of surface quantities like $L_W(\lambda)$ or $R_{rs}(\lambda)$.

The focus in this study is to establish the importance of data collection and processing to the total uncertainty within a combined above- and in-water perspective. These two sources of uncertainty express the principal differences in the above- and in-water protocols, because the other three are largely independent of either approach: the instruments are all calibrated the same way (standard lamps and plaques) and can be intercalibrated with the SQM to remove any calibration biases; one manufacturer is being used, so the in situ stability is usually within well-defined expectations; and all the sensors are exposed to the same oceanic and illumination environment. In such a framework, the latter three uncertainties are considered extraneous to the main objective. This is not to say they are insignificant—it is strictly an organizational expedient to clear away those problems that can be quantified expeditiously before the details of the primary objective are considered.

Calibration uncertainties were minimized by having the miniNESS, SeaSAS, DalSAS, and DalBOSS radiometers all calibrated at the same calibration facility (Satlantic) and at the same time. The monthly campaigns for the WiSPER radiometers did not permit them to be a part of the joint calibration exercise, so all the radiometers were intercalibrated using the SQM-II (section 3a). The SQM-II sessions were done in the field to also monitor the stability of the sensors while they were being deployed.

Environmental variability was minimized by only using data from simultaneous deployments of the instruments during the most stable solar illumination possible. The majority of the data were collected in Case-2 conditions, so the influence of the potentially increased heterogeneity of this type of environment was assessed (section 3b).

Data processing uncertainties were minimized by processing all the in-water data with one processor, and all the above-water data with one processor. The latter requires some common choices in filtering and sampling parameters; the importance of which are quantified below (section 3c) and then a single choice was made for all the above-water processing (section 4) where appropriate (the C85 method does not permit alternative processing parameters).

a. Sensor stability and intercalibration

SQM-II sessions were performed before, during, and after the field campaign. Although nine sessions were completed in total, only four were used for sensor intercalibration because of problems experienced with the SQM-II during shipping. Data collected during these four sessions show the SQM-II was stable to within 0.5% in the field. Nine of the thirteen radiometers were shown to be stable to within 1%, two were only tested in one session, and two were found to have at least one channel in the 2% range.

Most of the radiometers were calibrated before and after the experiment (between April 1998 and November 1998). The pre- and postcalibration values were compared as a percent change from the predeployment values. Most of the calibrations agreed to within 3% with the exception of I040, T069, Q33, and N48. The latter two still had so-called soft filters, which were shown to be a source of temporal instability (Hooker and Aiken 1998).

The individual radiometers were compared with the most stable sensor in each basic deployment category: in-water radiance, R035; in-air radiance, T09; in-water irradiance, I071; and in-air irradiance, M93 (Table 1). Because these baseline radiometers were stable to within 1% during the entire experiment, they were used to correct for any calibration variations (e.g., due to different lamps, setup error, plaque inhomogeneities, etc.), which can produce differences between calibrations on the order of 3%–5%. The mean of all the spectral radiometric data compared to the baseline radiometers to within 2%.

b. Environmental variability

The radiometric measurements were taken under different illumination conditions including fully overcast and cloud-free sky with sun zenith angles ranging from 11.5°–47.8°. The sea state was characterized by slight (0.1–0.5-m wave height) and moderate (0.5–1.25-m wave height) conditions producing a relatively wide range of variability in the sea surface roughness over the measurement days. According to the Loisel and Morel (1998) classification, the water was always close to the Case-1 and Case-2 separation threshold, but on SDY 191 and 195 it was classified as Case-2 with C_a values of 1.6 and 0.7 mg m^{-3}, respectively. On both days, the water column exhibited a strong optical stratification between the surface and 5-m depth. On SDY 194, the water was classified as Case-1 and was almost homogeneous from the surface to 12-m depth.

The lowest (0.08 m^{-1}) and the highest (0.32 m^{-1}) values of K_d were exhibited on clear days (SDY 194 and 191, respectively). Similarly, the sum of the particulate and dissolved organic matter beam attenuation coefficients ($c_p + c_y$) and the corresponding sum of the absorption coefficients ($a_p + a_y$) at 490 nm showed the lowest values on SDY 194 (0.55 and 0.03 m^{-1}, respectively) and the highest values on SDY 191 (2.14 and 0.16 m^{-1}, respectively).

The standard deviations in K_d, $a_p + a_y$, and $c_p + c_y$ indicate the daily variability in bio-optical parameters was, at times, appreciable. The effects of this variability on the in-water optical measurements were estimated by computing the standard deviations in $K_{L_u}(\lambda)$ and $L_u(0^-, \lambda)$, σ_K and σ_L, respectively. The standard de-

TABLE 4. A summary of some of the environmental characteristics of the AAOT site during the SeaBOARR-98 campaign. The K_d, $a_p + a_y$, and $c_p + c_y$ values are overall averages for the day and are given with one standard deviation as a percentage of the average. The Ångström exponent and coefficients are given by α and β, respectively (no data are shown for SDY 195 because of the overcast conditions). The values for $\sigma_K(\lambda)$ and $\sigma_L(\lambda)$ represent the minimum and maximum deviations (in percent of the average) of the standard deviations of K_{L_u} and L_u values from successive casts, respectively, over the 412–555-nm spectral range.

Environmental parameter	SDY 191	SDY 194	SDY 195
Water type[a]	Case-2	Case-1	Case-2
C_a [mg m^{-3}][b]	1.6	0.3	0.7
C_{TSM} [g m^{-3}][c]	2.8	0.8	1.9
K_d [m^{-1}][d]	0.32% ± 9.4%	0.08% ± 12.5%	0.23% ± 4.3%
$a_p + a_y$ [m^{-1}][e]	0.16% ± 7.7%	0.03% ± 3.8%	0.10% ± 2.0%
$c_p + c_y$ [m^{-1}][f]	2.14% ± 6.7%	0.55% ± 3.1%	1.26% ± 0.9%
Cloud cover (eighths)[g]	Clear (0/8)	Clear w/haze (0/8)	Overcast (8/8)
Illumination state[g]	Stable	Stable	Slightly changing
α, β[h]	1.6, 0.07	1.6, 0.15	
$\sigma_K(\lambda)$ [%][h]	1.5–1.8	1.2–2.0	1.5–1.7
$\sigma_L(\lambda)$ [%][h]	1.3–1.6	1.0–1.3	4.4–4.6
Solar zenith angle [°][g]	11.5–34.2	23.2–47.8	28.5–42.2
Water stratification[i]	Strong	None	Strong
Wind speed [m s^{-1}][g]	4.8	7.3	2.7
Sea roughness (state)[g]	Slight (1)	Moderate (1–2)	Slight (1)

[a] The Case-1 vs Case-2 distinction was determined using the Loisel and Morel (1998) classification scheme.
[b] Analyzed using the high performance liquid chromatography (HPLC) method (Joint Global Ocean Flux Study 1994 and Jeffrey et al. 1997).
[c] The total suspended matter (TSM) concentration, C_{TSM}, was obtained from the net weight of the material collected on GF/F filters following the technique of Strickland and Parsons (1972).
[d] Determined for $\lambda = 490$ nm.
[e] The in vivo spectral absorption coefficient of particulate matter retained on filters, $a_p(\lambda)$, was determined with a dual-beam spectrophotometer (Perkin Elmer Lambda 19) equipped with a 60-mm diameter integrating sphere (Tassan and Ferrari 1995), and the colored dissolved organic matter (or yellow substance) absorption coefficient, $a_y(\lambda)$, was determined using a (Perkin Elmer Lambda 12) dual-beam spectrometer (Ferrari et al. 1996); the reported values are for surface layer (0–1 m) samples and $\lambda = 490$ nm.
[f] The spectral attenuation $c(\lambda)$ (and absorption) of seawater particulate plus dissolved matter measured at nine wavelengths using a WETLabs, Inc. (Philomath, Oregon) AC-9 with a 25-cm pathlength; the reported values are for surface layer (0–1 m) samples and $\lambda = 490$ nm.
[g] A variety of meteorological observations or computations were made following World Meteorological Organization (WMO) guidelines including cloud cover, illumination state, sun position (zenith and azimuth), atmospheric pressure, relative humidity, air temperature, wind speed, and sea state; the latter conform to the WMO Code M scale (WMO–N.8).
[h] Derived from direct sun irradiance using a CE-318 sun photometer made by CIMEL Electronique (Paris, France).
[i] Derived from qualitative analysis of seawater temperature and salinity by CTD measurements plus AC-9 data.

viations were computed from successive, three-cast sequences of WiSPER measurements: three sequences on SDY 191, four on SDY 194, and two on SDY 195. The range in σ_K values were generally less than 2% at all wavelengths during all three days. The σ_L values were less than 2% on the clear sky days (SDY 191 and 194), but approximately 4.5% on the overcast day (SDY 195). The larger deviations for the latter are attributed to the variations in the illumination state (slightly changing). A summary of all the environmental parameters is given in Table 4.

c. Glint filtering and sampling

Figures 3–5 show the progression in data removal as the amount of glint filtering (Table 5) applied to a typical L_T time series is increased. The time series is DalSAS $L_T(490)$ data collected during SDY 194 (the only day when conditions were within the requirements of the NRSR workshop). As more and more of the large glint spikes are better delineated and removed, the final mean value of the $L_T(490)$ time series decreases from 1.92 (Fig. 3) to 1.83 (Fig. 4) and then finally to 1.77 (Fig. 5). The final (F_5) value represents approximately a 7.8% reduction with respect to the original (F_1) mean. It is important to note, there will be very little effect of increased filtering on data associated with calm sea surfaces, because the data will be relatively smooth (low variance).

Figure 6 shows the effect of glint filtering on the above-water methods using all the data for SDY 194—the only day when all methods are valid because it is during Case-1 conditions. In this case, the final $\hat{L}_W(\lambda)$ values for each filter were differenced with respect to an in-water $\tilde{L}_W^{S84}(\lambda)$ estimate from WiSPER data that was collected at the same time as the above-water data. The differences are reported as spectral averages (over the first five wavelengths), $\Psi_{S84}(\lambda_{1-5})$. The results show that the various above-water methods converge as more glint filtering is applied, and their agreement with the in-water measurement also converges with the use of more aggressive filtering.

M80: Filtering substantially improves agreement with the in-water estimate up to the point when sun glint spikes are significantly removed (F_2).

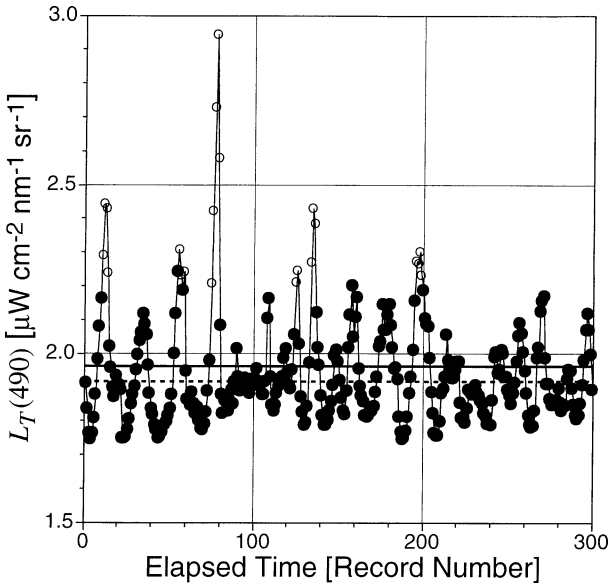

FIG. 3. A time series of $L_T(490)$ filtered using the original ocean optics protocols glint filter (F_1). The open circles are the data rejected by the filter, and the solid circles are those retained. Note that only the tips of the glint spikes are rejected by the filter. The solid horizontal line is the mean before data rejection, and the dashed line is the mean after.

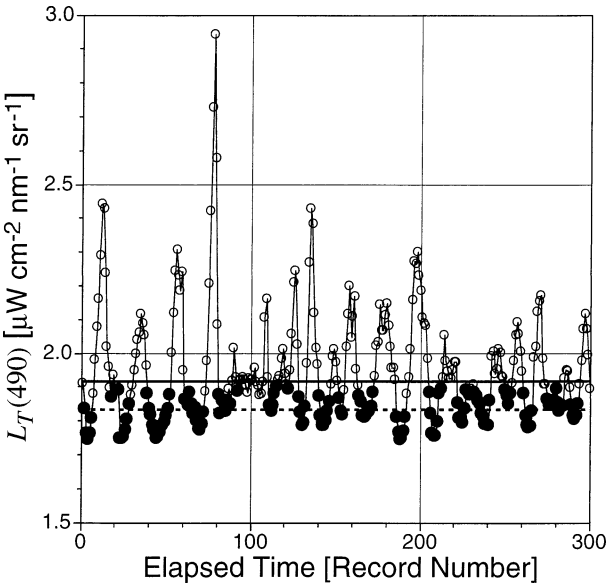

FIG. 4. The time series from Fig. 3 filtered using filter F_2. The solid horizontal line is the mean from filter F_1, and the dashed line is the mean after the application of filter F_2. Note that a much larger portion of the glint spikes are rejected by the filter (open circles), and that the retained data (solid circles) lie below the $L_T(490)$ estimated using filter F_1.

After that, increased filtering (and surface roughness) has a small effect in all bands except the 412-nm band (M80 is appropriate for rough sea surfaces). There is usually a small increase in $\Psi_{S84}^{M80}(\lambda_{1-5})$ beyond the F_5 result.

C85 : The method does not accommodate the notion of filtering, so there is no effect. The $\Psi_{S84}^{C85}(\lambda_{1-5})$ value remains a constant 10.7%.

S95: The effect of filtering is the largest, because S95 assumes a flat sea surface and does not account for residual reflection from surface waves. When surface roughness increases, the reflection from the waves does too, and because the method does not remove residual reflection, it tends to increasingly overestimate $\hat{L}_W$. Increased filtering removes not only sun glint spikes, but also the residual reflection, so the performance of the method improves continuously with more aggressive filtering. The best results are frequently obtained by using the minimum value, F_7. The $\hat{L}_W^{S95}$ value converges with the in-water $\hat{L}_W^{S84}$ estimates, but also very strongly with $\hat{L}_W^{M80}$ and $\hat{L}_W^{L98}$.

L98: The filtering results are the same as for M80.

Although the final three glint filters in Fig. 6 produced similar results, F_5 is the preferred filter because it retains some data for statistical consideration, whereas F_6 and F_7 do not. This is an important point because in the absence of having some amount of data for final analysis, the entire process might converge on a point that is simply noise, rather than a value that is indicative of the actual signal. Because of the significant improvement associated with the F_5 filter, all of the remaining above-water processing used this filter for glint removal unless otherwise indicated (C85 results always do not).

In terms of the stated performance of the S95 pro-

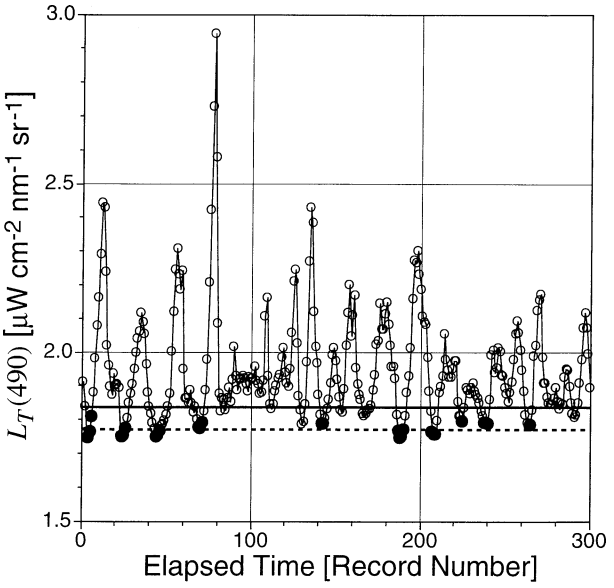

FIG. 5. The time series from Fig. 3 filtered using filter F_5. The solid horizontal line is the mean from filter F_2, and the dashed line is the mean after the application of filter F_5. Note that almost all of the data are rejected by the filter (open circles), and that the retained data (solid circles) lie at the very bottom of the glint troughs.

TABLE 5. A summary of the data filters used with the above-water techniques showing the filter code, the amount of data retained by the filter, and a generalized description of how the filtering technique is implemented.

Filter	Retention	Description of filtering technique
F_0	100%	All data accepted—no filtering.
F_1	~90%	Data values greater than $\mu + 1.5\sigma$ are removed (where μ is the mean and σ the standard deviation).
F_2	~50%	Data values greater than $\mu + 1.5\sigma$ are removed, a new mean is calculated from the remaining data, and then values greater than the new mean are removed.
F_3	~15%	Data points above the minimum value for which the coefficient of variance in the 490-nm band is less than 1.2% are accepted; if the number of accepted points is low, the lowest 15% of the total number of points are used.
F_4	~10%	The lowest 10% of the total number of data points based on the reddest (780-nm) band are kept.
F_5	~5%	The lowest 5% of the data, based on the reddest (780-nm) band, are kept.
F_6	<4%	The minimum value of L_T in each wavelength is determined, and then the spectra associated with the minimum values are averaged.
F_7	5 points	The minimum value of L_T at each wavelength is kept.

tocol, the implementation used here was different than the published methodology in one important respect: the filtering used (F_5) was more aggressive than originally proposed (F_1) or as subsequently revised (F_2). But because this filter was used with all of the methods except C85 (which uses averaging as part of the protocol), the intra- and intercomparison results are not biased. The results from the filtering analysis (Figs. 3–5) suggest if filtering is not considered carefully as part of the implementation of the methods, C85 will probably perform better than indicated here, and the other above-water methods (M80, S95, and L98) will perform significantly worse with respect to the in-water comparisons.

The use of 10-s averaging in the C85 method, and the fact that different sampling frequencies are a common part of field acquisition (SeaSAS had a 6 Hz sampling frequency, whereas DalSAS had a 10 Hz sampling frequency), suggests a more complete inquiry into sampling issues is appropriate. Figure 7 presents an analysis of 35 casts of SeaSAS $L_T(\lambda)$ data processed with the S95 method and the F_5 filter from SDY 194. The plot shows the effect of averaging and subsampling with respect to the original 6 Hz data; that is, $\Psi_{S95}(\lambda_{1-5})$ is the percent difference of the new (averaged or subsampled) result with respect to the original 6 Hz result. Although either modification to the original data density degrades performance, averaging is the most detrimental; a 10-s (0.1 Hz) subsampling produces on average a 1.1% increase and can range from −3.1% to 6.8%, whereas 10-s averaging produces on average an 8.3% increase and can range from 2.9% to 14.1%. The reason for the difference has to do with the discretization of the glint. Both types of smoothing reduce the amplitude and width of the glint spikes, but averaging spreads the energy of the glint into the background signal and elevates the final radiances; sub-

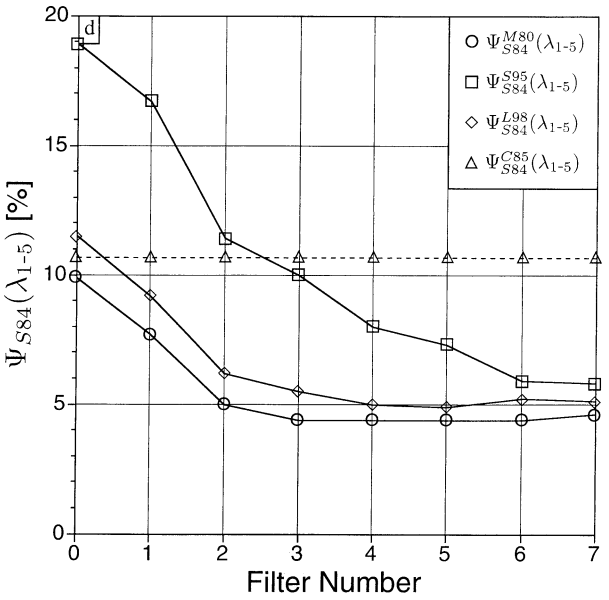

FIG. 6. The importance of glint filtering determined by calculating $\Psi(\lambda_{1-5})$ using S84 (with WiSPER data) plus M80, S95, L98, and C95 (all with DalSAS data) as a function of filters F_1–F_7 (F_0 is no filtering).

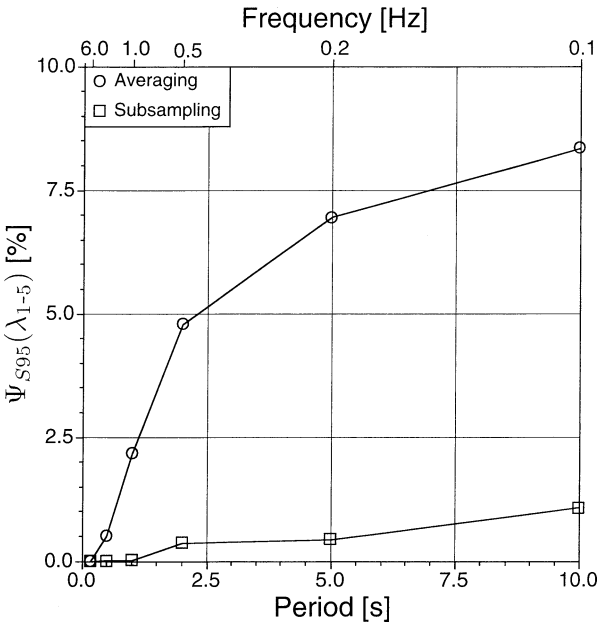

FIG. 7. The importance of averaging (circles) and subsampling (squares) determined by calculating $\Psi(\lambda_{1-5})$ using the S95 method and the F_5 filter on 35 casts of SeaSAS $L_T(\lambda)$ data from SDY 194.

sampling can only do this if the time series are very short. All above-water acquisition events lasted 3 min, so this is not a problem here.

4. Results

This study is concerned with an extensive set of experimental comparisons determined from above- and in-water radiometric measurements. Seven methods for deriving water-leaving radiances are computed from five instrument systems (Fig. 2) with five common wavelengths (Table 1) using data from two water types (Case-1 and Case-2), two categories of water stratification and sea surface roughness (Table 4), plus two illumination conditions (clear and overcast skies). Embedded within this already complicated data matrix are additional subtleties associated with the sampling systems and their respective protocols.

Recognizing that no one organizational scheme can compactly and succinctly present all of the data relationships, the presentation plan adopted here is to split the presentation into in-water intracomparisons (section 4a), above-water intracomparisons (section 4b), and above- and in-water intercomparisons (section 4c). To provide some commonality and easy cross-referencing between comparison categories, an overall synthesis is established first using spectral averages, which are then used to determine the areas of inquiry demanding greater analytical detail using band ratios and discrete wavelengths. Consequently, each comparison category has a separate section dealing with spectral averages, band ratios, and discrete wavelengths.

The results are presented primarily in tables rather than figures, so the quantitative values are immediately accessible. The tables are organized following the smaller-scale presentation scheme: spectral averages are presented first followed by the band-ratio and discrete wavelength results. Each table contains partitions for the various comparison products. Although this does not duplicate the larger-scale organization of above- and in-water intracomparisons followed by the intercomparisons of all methods, it keeps all like data products together and makes the discerning of comparative relationships relatively simple.

Table 6 presents the spectrally averaged comparisons of all of the methods for the three sampling days. The data are the $\Psi(\lambda_{1-5})$ values for the matrixed methods that are formed by taking a particular method, given as one of the columns, and comparing the water-leaving radiances from that method with another, given as one of the rows. Within each day, the upper right-most (triangular) side of the table presents the in-water intracomparisons, the bottom left-most (triangular) side presents the above-water intracomparisons, and the upper left-most (rectangular) portion presents the above- and in-water intercomparisons. The separate comparisons along the bottom (middle and right) of the daily results are for the same method applied to two different instrument systems.

The evolution in the analytical results are presented from a large- to small-scale perspective in Tables 7–9. Table 7 displays average comparisons across the appropriate methods or instruments (shown in Table 6) for each day and for all days. The method averages quantify the overall performance of each method with respect to the others, while the instrument averages provide greater detail in instrument and protocol sampling issues. Table 8 gives the 490- and 555-nm band-ratio results ($\Phi_{3/5}$) for the analyses presented in Table 7.

All the computations in Tables 6–8 are derived from the maximum number of simultaneous casts for each comparison. Consequently, the number of data points in the averages changes from method to method, and from day to day. Tables 6–8 also give the standard deviations associated with the averages, which are an indicator of any spectral dependence in the comparisons, but a detailed inquiry into the discrete wavelengths of the comparisons is presented in Table 9. To manage the complexity in the presentation, only the S84 (WP) data is used for the latter comparisons. This is an appropriate choice because the WiSPER data has the best sampling density of the in-water data, and the majority of the data were collected in Case-2 conditions where vertical resolution needs to be maximized. The significance of this point is well demonstrated by Hooker et al. (2001).

a. In-water intracomparisons

The comparisons within the group of in-water methods involve the same method applied to two different instruments, and multiple methods applied to different instruments. In both cases, spectral averages and band-ratio averages are used to focus in on the dominant relationships, and then a discrete wavelength analysis is used to reveal any spectral dependence in the latter.

1) SPECTRAL AVERAGES

The first in-water intracomparisons to be considered are the S84 spectral averages derived from simultaneous deployments of the miniNESS and WiSPER instruments (these results appear as separate intersections along the right-most, bottom edge of the daily entries in Table 6). The miniNESS data are from time periods when the profiler was deployed 7.5 m from the tower (the same distance as the WiSPER system). These intracomparisons set a minimum level of agreement for the in-water methods, because the sampling occurred within close proximity to one another, and the same method was used to process the data.

During case-1 conditions (SDY 194), the uncertainty between the two instruments is to within 3.4%, which is in keeping with the Hooker and Maritorena (2000) case-1 (open ocean) results. During case-2 conditions (SDY 191 and 195), however, the uncertainty increases (on average) by about a factor of 2 to approximately 7.8%, and the overall uncertainty (across all three days) is at the 6.3% level (Table 7b). The degradation in agreement is

TABLE 6. Comparisons of above- and in-water methods as a function of the three sampling days (a) SDY 191, (b) SDY 194, and (c) SDY 195. The listed values are the $\bar{\psi}$ spectral averages, i.e., over the first five wavelengths; the numbers in parentheses are the standard deviations in the spectral averages. The intracomparisons are the intersections of like methods with one another (in-water vs in-water or above-water vs above-water), and the intercomparisons are the intersections of different methods (in-water vs above-water). Intracomparisons using the same method but different data streams, i.e., S95 calculated from SeaSAS (SS) and DalSAS (DS) data plus S84 calculated from miniNESS (MN) and WiSPER (WP) data, are shown separately for each day. The entries shown in bold face indicate methods not formulated for Case-2 conditions, e.g., the P97 method calculated from DalBOSS (DB) data on SDY 191 and 195. It is important to remember the overall environmental conditions for each day (Table 4), in particular, SDY 191 and 194 were clear sky, and SDY 195 was overcast. The *N* values are the number of data points in the averages (the number of casts times 5).

(a) Case-2	N = 30–45 Above-water methods				N = 60 In-water methods		
SDY 191	L98 (DS)	M80 (DS)	C85 (DS)	S95 (DS)	P97 (DB)	P94 (DB)	S84 (WP)
S84 (WP)	**13.1 (7.8)**	**17.0 (12.1)**	3.3 (2.6)	3.2 (2.5)	**10.9 (8.1)**	9.3 (2.1)	
P94 (DB)	**16.3 (3.7)**	**20.9 (6.2)**	7.5 (2.9)	6.5 (2.6)	**16.5 (2.9)**		
P97 (DB)	**3.8 (2.7)**	**7.2 (5.0)**	**10.9 (5.8)**	**12.1 (5.4)**			
S95 (DS)	**12.4 (4.6)**	**16.4 (9.6)**	1.2 (0.4)				
C85 (DS)	**11.3 (4.9)**	**15.2 (10.0)**					
M80 (DS)	**4.2 (5.3)**		N = 50	S95 (DS)		N = 20	S84 (WP)
L98 (DS)			S95 (SS)	2.0 (1.1)		S84 (MN)	6.3 (4.6)
(b) Case-1	N = 40–50 Above-water methods				N = 45–50 In-water methods		
SDY 194	L98 (DS)	M80 (DS)	C85 (DS)	S95 (DS)	P97 (DB)	P94 (DB)	S84 (WP)
S84 (WP)	4.4 (3.1)	3.8 (2.9)	9.8 (4.0)	6.0 (4.2)	6.3 (6.8)	5.9 (5.8)	
P94 (DB)	6.1 (4.7)	4.9 (3.7)	12.1 (6.3)	6.4 (4.8)	2.3 (1.8)		
P97 (DB)	6.3 (5.5)	4.6 (4.3)	12.0 (7.4)	6.5 (5.5)			
S95 (DS)	8.9 (3.1)	7.7 (3.2)	3.5 (2.2)				
C85 (DS)	12.4 (2.0)	11.1 (3.8)					
M80 (DS)	3.0 (2.0)		N = 100	S95 (DS)		N = 65	S84 (WP)
L98 (DS)			S95 (SS)	9.2 (5.1)		S84 (MN)	3.4 (2.2)
(c) Case-2	N = 20–40 Above-water methods				N = 25–50 In-water methods		
SDY 195	L98 (DS)	M80 (DS)	C85 (DS)	S95 (DS)	P97 (DB)	P94 (DB)	S84 (WP)
S84 (WP)	**7.6 (6.1)**	**6.6 (5.4)**	8.0 (5.5)	10.3 (5.9)	**9.9 (7.0)**	7.4 (5.8)	
P94 (DB)	**6.9 (5.6)**	**10.3 (6.1)**	11.7 (6.4)	5.1 (4.0)	**7.8 (2.8)**		
P97 (DB)	**11.1 (7.6)**	**16.6 (5.8)**	**18.0 (6.1)**	**10.6 (5.1)**			
S95 (DS)	**4.7 (3.4)**	**7.7 (5.4)**	5.9 (4.0)				
C85 (DS)	**5.4 (3.9)**	**1.8 (1.5)**					
M80 (DS)	**6.7 (5.2)**		N = 30	S95 (DS)		N = 10	S84 (WP)
L98 (DS)			S95 (SS)	16.4 (9.5)		S84 (MN)	9.3 (6.6)

due to the added complexity of Case-2 waters, and in particular, the strong stratification during SDY 191 and 195. The latter is important because the stratification was restricted to the uppermost part of the water column, and the two instruments did not sample this interval equally: WiSPER was slowly raised and lowered through the water column, so it collected a large number of near-surface samples; miniNESS fell freely and (comparatively) quickly through the water column, so the near-surface sampling was more coarse. An additional source of uncertainty was the degraded stability of the illumination field during the overcast conditions on SDY 195.

The intracomparison of the other two in-water methods (which used the same instrument), the intersection of P94 (DB) and P97 (DB) in Table 6, agree to within approximately 2.3% during Case-1 conditions, and (on average) to within about 12.2% during Case-2 conditions. The P94 method uses $K_{L_u}(\lambda)$ estimated from miniNESS data, however, so these results are not independent of the S84 analysis with WiSPER and miniNESS data. The agreement between P94 and P97 on SDY 194 is better than expected and is an artifact of the model used with P97 (Morel 1988). On this day, the modeled $K(\lambda)$, actually $K_d(\lambda)$, agreed very closely with the in situ $K_{L_u}(\lambda)$ results from miniNESS, so they compare unexpectedly well.

The SQM-II baseline radiometer data were used as a correction for the other sensors, and reduced the radiometric uncertainty in the data to the 1%–2% level. All data products were produced using the same processor, except the WiSPER data. The intercomparison of these data with miniNESS data taken at the same distance

TABLE 7. The comparison of above- and in-water methods based on the $\bar{\psi}$ values presented in Table 6: (a) the overall spectral averages for the individual above- and in-water intracomparisons, i.e., the $\bar{\Psi}$ values for one above-water method compared to all the other above-water methods or one in-water method compared to all the other in-water methods; (b) the individual spectral averages ($\bar{\psi}$) from two above- and in-water instruments using the same method, in this case, S95 (SS and DS) for the former and S84 (WP and MN both at 7.5 m) for the latter; (c) the overall spectral averages for all the above- and in-water intracomparisons; and (d) the overall spectral averages for all the above- and in-water intercomparisons. The entries shown in bold face indicate methods unsuitable for Case-2 conditions (SDY 191 and 195). The values in parentheses are the standard deviations in the averaged values. The averages and standard deviations across all three days or all methods (the All entries) were computed by assuming each daily or method entry was an independent measure of performance. The Range values were formed by subtracting and adding one standard deviation to the averages from the All entries.

	Above-water intracomparisons				In-water intracomparisons		
(a) SDY	L98 (DS)	M80 (DS)	C85 (DS)	S95 (DS)	P97 (DB)	P94 (DB)	S84 (SP)
191 (Case-2)	**9.3 (4.9)**	**12.0 (8.6)**	9.2 (6.4)	10.0 (6.2)	**13.7 (6.1)**	12.9 (2.6)	10.1 (5.9)
194 (Case-1)	8.1 (2.4)	7.3 (3.1)	9.0 (2.8)	6.7 (2.9)	4.2 (4.8)	4.0 (4.2)	6.1 (6.3)
195 (Case-2)	**5.6 (4.2)**	**5.4 (4.4)**	4.4 (3.3)	6.1 (4.4)	**8.3 (4.6)**	7.5 (4.0)	8.6 (6.4)
All	*7.7 (4.0)*	*8.2 (5.8)*	*7.5 (4.5)*	*7.6 (4.7)*	*8.7 (5.2)*	*8.1 (3.6)*	*8.3 (6.2)*
Range	*3.7–11.7*	*2.4–14.0*	*3.0–12.0*	*2.9–12.3*	*3.5–13.9*	*4.5–11.7*	*2.1–14.5*

	S95 (DS and SS)			S84			
(b) SDY	Both	Opposite	Same	(WP and MN)	(c) SDY	Above-water	In-water
191 (Case-2)	2.0 (1.1)	2.1 (1.2)	1.7 (1.0)	6.3 (4.6)	191	10.1 (6.6)	12.2 (5.1)
194 (Case-1)	9.2 (5.1)	14.1 (3.8)	6.1 (2.8)	3.4 (2.2)	194	7.8 (2.8)	4.8 (5.2)
195 (Case-2)		16.4 (9.5)		9.3 (6.6)	195	5.4 (4.1)	8.1 (5.1)
All	*5.6 (3.7)*	*10.9 (5.9)*	*3.9 (2.1)*	*6.3 (4.8)*	All	*7.8 (4.8)*	*8.4 (5.1)*
Range	*7.8–11.6*	*5.0–16.8*	*1.8–6.0*	*1.5–11.1*	Range	*3.0–12.6*	*3.1–13.5*

	Above- and in-water intercomparisons					
(d) All Days	L98 (DS)	M80 (DS)	C85 (DS)	S95 (DS)	All	Range
S84 (WP)	8.4 (6.0)	9.2 (7.8)	7.0 (4.2)	6.5 (4.4)	*7.7 (5.8)*	*1.9–13.5*
P94 (DB)	9.8 (4.7)	12.0 (5.5)	10.5 (5.5)	6.0 (3.9)	*9.6 (4.9)*	*4.7–14.5*
P97 (DB)	7.1 (5.7)	9.5 (5.0)	13.7 (6.4)	9.7 (6.4)	*10.0 (5.9)*	*4.1–15.9*
All	*8.4 (5.5)*	*10.2 (6.2)*	*10.4 (5.5)*	*7.4 (5.0)*	*9.1 (5.6)*	
Range	*2.9–13.9*	*4.0–16.4*	*4.9–15.9*	*2.4–12.4*	*3.5–14.7*	

TABLE 8. The comparison of above- and in-water methods based on the band-ratio, $\Phi_{3/5}$, analyses. The presentation and techniques follow those used in Table 7.

	Above-water intracomparisons				In-water intracomparisons		
(a) SDY	L98 (DS)	M80 (DS)	C85 (DS)	S95 (DS)	P97 (DB)	P94 (DB)	S84 (WP)
191 (Case-2)	**3.5 (0.4)**	**3.9 (0.6)**	3.6 (0.4)	3.5 (0.4)	**4.6 (0.6)**	2.6 (0.7)	3.3 (0.7)
194 (Case-1)	0.8 (0.5)	0.7 (0.4)	1.0 (0.4)	0.9 (0.4)	3.5 (0.4)	4.7 (0.4)	6.0 (0.6)
195 (Case-2)	**0.8 (0.5)**	**0.9 (0.6)**	0.6 (0.4)	0.7 (0.6)	**5.4 (0.6)**	4.0 (0.6)	5.6 (1.0)
All	*1.7 (0.4)*	*1.8 (0.5)*	*1.8 (0.4)*	*1.7 (0.4)*	*4.5 (0.6)*	*3.8 (0.6)*	*5.0 (0.8)*
Range	*1.3–2.1*	*1.3–2.3*	*1.4–2.2*	*1.3–2.1*	*3.9–5.1*	*3.2–4.4*	*4.2–5.8*

	S95 (DS and SS)			S84			
(b) SDY	Both	Opposite	Same	(WP and MN)	(c) SDY	Above-water	In-water
191 (Case-2)	3.5 (2.7)	5.6 (0.6)	0.4 (0.3)	7.2 (0.7)	191	3.6 (0.5)	3.5 (0.7)
194 (Case-1)	5.1 (1.2)	6.4 (0.7)	4.2 (0.5)	1.7 (0.6)	194	0.9 (0.4)	4.7 (0.5)
195 (Case-2)		4.2 (1.0)		12.0 (2.1)	195	0.8 (0.5)	5.0 (0.8)
All	*4.3 (2.1)*	*5.4 (0.8)*	*2.3 (0.4)*	*7.0 (1.3)*	All	*1.7 (0.5)*	*4.4 (0.6)*
Range	*2.2–6.4*	*4.6–6.2*	*1.9–2.7*	*5.7–8.3*	Range	*1.2–2.2*	*3.8–5.0*

	Above- and in-water intercomparisons					
(d) All Days	L98 (DS)	M80 (DS)	C85 (DS)	S95 (DS)	All	Range
S84 (WP)	3.9 (1.7)	3.3 (1.5)	1.5 (1.3)	1.8 (0.9)	*2.7 (1.4)*	*1.3–4.1*
P94 (DB)	5.7 (1.4)	3.8 (0.8)	2.3 (0.6)	2.4 (0.5)	*3.5 (0.9)*	*2.6–4.4*
P97 (DB)	7.2 (1.6)	5.1 (0.7)	3.2 (0.7)	3.6 (0.7)	*4.8 (1.0)*	*3.8–5.8*
All	*5.6 (1.6)*	*4.1 (1.0)*	*2.3 (0.9)*	*2.6 (0.7)*	*3.7 (1.1)*	
Range	*4.0–7.2*	*3.1–5.1*	*1.4–3.2*	*1.9–3.3*	*2.6–4.8*	

TABLE 9. The average discrete wavelength comparisons for the S84 (left-most five wavelengths) and S95 methods (right-most five wavelengths) with respect to the other methods as a function of the sampling day and for all days.

	S84 comparisons						S95 comparisons					
SDY	Method	$\bar{\psi}$ (412)	$\bar{\psi}$ (443)	$\bar{\psi}$ (490)	$\bar{\psi}$ (510)	$\bar{\psi}$ (555)	Method	$\bar{\psi}$ (412)	$\bar{\psi}$ (443)	$\bar{\psi}$ (490)	$\bar{\psi}$ (510)	$\bar{\psi}$ (555)
191 (Case-2)	P94	9.1	11.3	9.2	9.1	7.8	P94	5.4	5.7	5.9	9.7	6.0
194 (Case-1)		16.6	3.8	1.4	1.6	6.4		13.7	4.4	3.3	1.3	9.4
195 (Case-2)		10.9	8.7	6.1	7.0	4.4		9.1	6.2	3.9	2.1	4.0
All		*12.2*	*7.9*	*5.5*	*5.9*	*6.2*		*9.4*	*5.4*	*4.4*	*4.4*	*6.5*
191 (Case-2)	P97	**24.9**	**4.1**	**6.2**	**8.0**	**11.4**	P97	**21.0**	**9.4**	**9.6**	**7.5**	**13.2**
194 (Case-1)		19.0	3.5	2.6	3.0	3.6		16.2	5.5	3.0	1.1	6.6
195 (Case-2)		**18.4**	**6.6**	**7.6**	**7.0**	**9.8**		**15.4**	**10.0**	**8.7**	**6.4**	**12.6**
All		*20.7*	*4.7*	*5.5*	*6.0*	*8.3*		*17.5*	*8.3*	*7.1*	*5.0*	*10.8*
191 (Case-2)	S95	5.8	2.9	1.8	2.7	2.7	S84	5.8	2.9	1.8	2.7	2.7
194 (Case-1)		2.9	10.2	5.8	3.9	7.5		2.9	10.2	5.8	3.9	7.5
195 (Case-2)		9.2	15.1	9.7	8.2	9.6		9.2	15.1	9.7	8.2	9.6
All		*6.0*	*9.4*	*5.7*	*4.9*	*6.6*		*6.0*	*9.4*	*5.7*	*4.9*	*6.6*
191 (Case-2)	M80	**38.1**	**19.1**	**11.0**	**12.6**	**4.2**	M80	**32.0**	**21.5**	**12.2**	**9.6**	**6.7**
194 (Case-1)		7.4	4.2	2.5	2.5	2.6		10.7	8.4	6.2	6.3	7.1
195 (Case-2)		**4.6**	**15.4**	**5.8**	**3.0**	**4.3**		**10.9**	**9.0**	**6.9**	**6.1**	**5.8**
All		*16.7*	*12.9*	*6.4*	*6.0*	*3.7*		*17.9*	*13.0*	*8.4*	*7.3*	*6.5*
191 (Case-2)	C85	6.2	2.7	1.9	4.3	1.4	C85	0.5	1.2	1.3	1.4	1.4
194 (Case-1)		7.7	15.8	9.2	6.3	9.9		6.3	4.6	2.7	2.1	1.7
195 (Case-2)		6.8	16.9	6.8	4.0	5.4		24.1	9.6	11.8	12.2	15.0
All		*6.9*	*11.8*	*6.0*	*4.9*	*5.6*		*10.3*	*5.2*	*5.2*	*5.2*	*6.0*
191 (Case-2)	L98	**25.7**	**12.7**	**10.4**	**13.1**	**4.0**	L98	**19.4**	**14.9**	**11.4**	**10.0**	**6.4**
194 (Case-1)		5.0	4.7	2.7	7.1	2.4		7.4	7.9	8.8	12.0	9.0
195 (Case-2)		**6.1**	**13.0**	**6.8**	**5.9**	**5.9**		**6.5**	**5.5**	**3.9**	**4.0**	**3.8**
All		*12.3*	*10.1*	*6.6*	*8.7*	*4.1*		*11.1*	*9.4*	*8.0*	*8.7*	*6.4*

from the tower is approximately at the 3.4% level during optimal conditions (SDY 194). Given the size of the intercalibration uncertainty, this suggests the uncertainty associated with having two in-water data processors is on the order of 1%–2%. The environmental contribution to the uncertainty in the results was estimated to be 1%–3%, depending on the illumination conditions and the water type (Table 4).

Taking these three sources of uncertainty independently, and evaluating them as quadrature sums, the total uncertainty for nonmethodological sources is about 3%–4% from a spectral average point of view (for comparisons not involving WiSPER, the range would be about 2%–3%). This means agreement below this level is unnatural in the sense that it is better than expected. It can occur, however, if uncertainties cancel rather than sum, or if one or more of the assumptions associated with the formulation of a method are not realized in the data. For example, in the P97 formulation, the model agreed closer to the data than observational uncertainty would normally allow.

The basic capabilities of the in-water methods are derived from the intracomparison of all three methods. The lowest uncertainties are most frequently associated with the S84 method, and the largest uncertainties with the P97 method (Table 7a). The methods produce a relatively small range in Ψ values for each day: 9.3%–16.5% (SDY 191), 2.3%–6.3% (SDY 194), and 7.4%–9.9% (SDY 195). The differences between the methods are smaller in Case-1 conditions and larger in Case-2 conditions (by approximately a factor of 2), although, the standard deviation in the differences are in general similar (Tables 7b and 7c).

Because of the good performance of the WiSPER data, and the fact that P94 uses miniNESS data as part of the method, the remainder of the comparisons do not include miniNESS estimates of $\tilde{L}_w(\lambda)$ except for inquiries requiring two instruments and one processing method. It is important to remember the P94 and P97 methods do not include tower-shading effects, so the uncertainties between these methods alone are a few percent lower than with respect to the S84 (WP) comparisons.

2) BAND RATIOS

Table 8a presents the intracomparison of the in-water methods in terms of the 490- and 555-nm band ratio. The primary difference between these results and the average spectral results (Table 7a) are as follows:

1) the overall average differences, standard deviations, and ranges for all three days (the bottom two lines) are smaller with most of the results within 5%;
2) almost all of the individual differences and standard deviations are significantly smaller (the standard deviations are at the 1% level or less);
3) the P94 and S84 in-water methods intracompare best during Case-2 conditions (the best results for P97 are achieved in Case-1 waters); and

4) even though P97 is not designed for Case-2 waters, the band-ratio differences for this method are below or close to the 5% level during Case-2 days.

The best in-water method is P94, although all methods have an average difference across all three days of 5% or less.

The band-ratio results for using the same in-water method with two different instruments are presented in Table 8b. With respect to the average spectral results (Table 7b), there is improvement during Case-1 conditions (SDY 194), but the Case-2 values are sufficiently degraded that the effect is a deterioration in the overall average agreement from 6.3% to 7.0%. The standard deviations are smaller for the band-ratio approach, so the net effect is a smaller range of expected differences and, thus, a net improvement.

The overall intracomparison averages using the band-ratio approach are given in Table 8c. All of the daily differences and standard deviations are smaller than the average spectral results (Table 7c). Most notably, the in-water results are only significantly improved during Case-2 conditions; across all three days, the overall average is below 5% (which represents a factor of 1.9 improvement over the average spectral results); and the best agreement occurs during Case-2 conditions.

A repeat of the uncertainty analyses performed for the average spectral results [section 4a(1)] indicates the nonmethodological (calibration, environment, etc.) uncertainty range for the band-ratio data is about 2%–3% for comparisons involving WiSPER data (which used a different data processor) and 1%–2% for all others. If these values are considered against the overall averages, approximately 1%–3% of the total uncertainty budget can be attributed to differences in the methods.

3) DISCRETE WAVELENGTHS

The discrete wavelength, in-water intracomparisons for the S84 method are given in Table 9 (top two methods, left-most five wavelengths). Several uncertainties are less than 5%, and a few are to within 3%, although only for Case-1 conditions. The largest uncertainties are found in the blue domain (particularly 412 nm), but large uncertainties are also seen in the green wavelengths for all conditions. The largest uncertainties are found with the P97 results, for which there is a notable degradation in performance during Case-2 conditions (as expected, because P97 is not formulated for Case-2 waters).

b. Above-water intracomparisons

The comparisons within the group of above-water methods follow the same basic scheme adopted for the in-water methods: the same method is applied to two different instruments, but the evaluation of multiple methods involves the use of a single instrument. Again, spectral averages and band-ratio averages are used to focus in on the dominant relationships, and then a discrete wavelength analysis is used to reveal any spectral dependence in the latter.

1) SPECTRAL AVERAGES

The first above-water intracomparisons to be considered are the S95 results derived from simultaneous casts of the DalSAS (DS) and SeaSAS (SS) instruments (these results appear as separate intersections along the bottom, middle edge in the daily entries of Table 6). These comparisons set a minimum level of agreement for the above-water methods because the sampling occurred within close proximity, and the same method was used to process the data (bottom reflection and tower-shading corrections were not removed from either dataset). During Case-1 conditions (SDY 194), the two instruments agree to within approximately 9.2%, but during Case-2 conditions, they agree either very well, 2.0% on SDY 191, or very poorly, 16.4% on SDY 195. The variability in the latter might be due to the added complexity of Case-2 waters, but it could also be sensitivity to another variable (e.g., SDY 195 was overcast with slightly changing illumination and nonuniform distribution of sky radiance).

The intracomparison of the other above-water methods using DalSAS data (the intersections of L98, M80, and C85 with one another in Table 6) also exhibit dissimilar ranges in uncertainties with respect to water type: approximately 3.0%–12.4% during Case-1 conditions (SDY 194), and about 4.2%–15.2% (SDY 191) and 1.8%–6.7% (SDY 195) during Case-2 conditions. There is an inverse relationship between using the same instrument versus using different instruments: when one exhibits low average values, the other exhibits high values. From the point of view of either set of data, the two Case-2 days appear much different, which suggests a greater sensitivity in the above-water methods to the Case-2 conditions considered here. Another explanation is the above-water methods are sensitive to other variables, such as surface roughness and sky conditions.

The intracomparison of all the above-water methods establishes the basic capabilities of the above-water methods with respect to one another (this is a simpler comparison than the in-water exercise because, in this case, all of the methods use the same data). The methods produce a large range in uncertainties for each day except for the last day (Case-2 conditions): 1.2%–16.4% (SDY 191), 3.0%–12.4% (SDY 194), and 1.8%–7.7% (SDY 195). Very low uncertainties can be found on all days, but the methods associated with the smallest uncertainty changes from day to day: S95 and C85 on SDY 191, M80 and L98 on SDY 194, and C85 and M80 on SDY 195. The persistently lowest values are most frequently associated with the C85 and S95 methods, and the highest values are usually seen with the M80 method. Although this is reflected in the overall

averages in Table 7a, the intracomparison uncertainties are similar for all methods across all conditions.

There remains the problem of reconciling these basic results with the above-water analyses involving one method but two instruments, which is considered in more detail in Table 7b. Because two deployment sites were used with DalSAS (Fig. 1), there were times when it viewed the sea surface in the same azimuthal direction (with respect to the sun) as SeaSAS, and there were times when it viewed the opposite direction (i.e., one instrument was pointed at ϕ^+ and the other at ϕ^-). From the perspective of the S95 method, both viewing angles satisfy the protocol, but the data in Table 7b shows they do not produce similar estimates of $\hat{L}_w(\lambda)$. When the two instruments were pointed in the same direction, they agree to within 3.9%; when they were pointed in opposite directions, the agreement deteriorates to 10.9% (note the better agreement on SDY 191 when the sea surface was not very rough). The difference is approximately 7.0%, which is almost equal to the general performance of the above-water methods across all three days of sampling (Table 7c).

2) BAND RATIOS

The general conclusion seen with the in-water band-ratio analysis—that the average differences, standard deviations, and ranges are reduced with respect to the average spectral analysis results—is more significantly expressed with the above-water band-ratio results (Table 8a). The smallest differences are seen during SDY 194 and 195 which correspond to Case-1 and Case-2 water types, respectively, although, the latter was an overcast day. The best above-water method is S95 (and L98), although all of the methods have an average difference across all three days below 2% and standard deviations at about 0.5%. It is important to remember all of the Table 8a intracomparisons involve one instrument (DalSAS).

The band-ratio results for using the same above-water method with two different instruments are presented in Table 8b. With respect to the spectral results (Table 7b), there is an overall improvement in the above-water values. Although there is still evidence of a discrepancy in the above-water data for when the instruments were pointed in the same or opposite directions, the difference is not as large: 3.1% for the band-ratio results versus 7.0% for the spectral analysis. The large reduction in the standard deviations, however, makes this more significant than just the change in the average differences would suggest.

The overall intracomparison averages using the band-ratio approach (Table 8c) show substantial improvements in these data with respect to the spectral results (Table 7c): (a) for each day, the average differences and standard deviations are significantly lower in comparison to the spectral results; and (b) across all three days, the overall average is less than 2% (this represents a factor of 4.6 improvement over the spectral results). Interestingly, the best agreement occurs during (overcast) Case-2 conditions (although, the Case-1 results are very similar). The very low percent differences (below 1%) for the above-water results during SDY 194 and 195 suggest some of the nonmethodological uncertainties discussed earlier are cancelling out rather than summing up (even with the rougher sea surface on SDY 194).

The biggest difference between the spectral and band-ratio results, in terms of how the methods are ranked (best to worst), occurs with the C85 and L98 methods. In the spectral results, L98 intracompared much better than C85, but in the band-ratio results, the reverse is true. The other unusual result is that the M80 and P97 methods, which were not formulated for Case-2 conditions, yield overall average differences less than 2%.

3) DISCRETE WAVELENGTHS

The above-water intracomparisons for the S95 method in terms of discrete wavelengths are given in Table 9 (bottom three methods, right-most five wavelengths). There is a general trend of maximum uncertainties in the blue domain for the M80 and L98 intracomparisons during clear sky conditions (SDY 191 and 194) which decrease through the green wavelengths. For overcast conditions (SDY 195) and for the C85 intracomparisons, the uncertainties are spectrally flatter. There are comparisons below the 5% level for the L98 and C85 methods, but the only uncertainties to within 3% occur for the latter.

c. Above- and in-water intercomparisons

The intracomparisons establish the capabilities of the above- and in-water methods separately, but the utility of the methods for calibration and validation exercises requires a demonstrated intercomparison uncertainty to within 5%, and preferably to approximately 3%.

1) SPECTRAL AVERAGES

The intercomparison of the above- and in-water methods is presented in the upper (left-most), rectangular boxes for the daily categories in Table 6. Some general relationships are immediately apparent.

1) The largest differences and standard deviations are associated with Case-2 conditions, although the smallest differences and standard deviations are also associated with Case-2 waters.
2) During each day, there is a lot of variability as to which methods intercompare with the smallest and largest differences, but the range in uncertainties between Case-1 (3.8%–12.1% for SDY 194) and Case-2 (3.2%–20.9% for SDY 191 and 5.1%–18.0% for SDY 195) conditions are, nonetheless, distinct.

3) The best methods change from day to day (S95 and S84 on SDY 191, M80 and S84 on SDY 194, and S95 and P94 on SDY 195), but it most frequently involves S84 and S95.
4) Even methods not formulated for the Case-2 environment are capable of producing differences (and standard deviations) in keeping with results achieved in Case-1 conditions.

It is important to remember the P94 and P97 methods do not include tower-shading effects, so the uncertainties between these methods and all the other methods include this extra source of variance.

Intercomparisons below or near the 5% limit occur for all three days (Table 6), although, almost all of these are associated with the clear-sky days (SDY 191 and 194). The overall averages for the intercomparisons are above the 5% level (Table 7d), but these are the most appropriate data for ranking the performance of the methods. The best above-water method is S95, because it has the smallest average difference, standard deviation, and range in expected differences across all the methods. The worst above-water method is C85, although M80 exhibits a similar range (because of a lower average difference but a higher standard deviation). The best in-water method is S84, although, P94 has a similar range (because of a smaller standard deviation).

The S95 and S84 methods were also the two best performers in terms of the intracomparison analyses. The overall intercomparison of these two methods (Table 7d) has an average difference and standard deviation of 6.5% and 4.4%, respectively. Considering this encompasses Case-1 and Case-2 conditions plus a significant part of the SeaWiFS spectrum (412–555 nm), this is an encouraging result. If all the methods are considered as one group, the average difference is 9.1% with a standard deviation of 5.6%.

2) BAND RATIOS

The band-ratio intercomparison results are shown in Table 8d. There is a significant improvement in the average differences and standard deviations with respect to the spectral averages (Table 7d), and almost all of the individual intercomparisons are below the 5% level, and many are to within 3%. Across all methods, the best and worst above-water methods are C85 and L98, respectively. Note that the results for the S95 method are only marginally worse than the C85 method. The best and worst in-water methods are S84 and P97, respectively. The overall average and standard deviation is 3.7% and 1.1%, which is approximately 2.5 and 5.1 times smaller, respectively, than the corresponding spectral averages.

3) DISCRETE WAVELENGTHS

The above- and in-water intercomparisons for the S84 and S95 methods are given in Table 9 (bottom four methods, left-most five wavelengths, and top three methods, right-most five wavelengths, respectively). The S95 and S84 intercomparisons appear twice because these are the selected comparators for both types of measurements. The spectral dependence in the S95 and S84 intercomparisons is notable at 510 nm, which is a persistent minimum with higher uncertainties above and below, and at 443 nm, which stands out as large maximums. Agreement to within 5% is achieved on SDY 194 and agreement to within 3% is found for almost all of the wavelengths on SDY 191.

The P94 results show a small decrease in uncertainties with increasing wavelength from 443 to 510 nm. The most notable results are the elevated uncertainties at 412 and 555 nm. The P97 values are similar, except the magnitude of the behavior is larger, particularly during Case-2 conditions.

The M80 and L98 results show a general trend of maximum uncertainties in the blue part of the spectrum that decreases with increasing wavelength during Case-2 conditions. During Case-1 conditions, the M80 and L98 results are spectrally flatter. Agreement to within 5% is found on all three days, except for L98 on SDY 195 (which was overcast) and C85 on SDY 194. The best results occur for Case-1 conditions with many uncertainties below 3%. The C85 values are also spectrally flatter, except for the elevated uncertainties at 443 nm.

5. Discussion

Three types of comparisons were used to evaluate above- and in-water methods for determining water-leaving radiances: spectral averages of the first five SeaWiFS wavelengths (Tables 6 and 7), the ratio of the water-leaving radiances in the 490- and 555-nm channels (Table 8), and discrete wavelengths in the 412–555-nm range (Table 9). All were quantified using the UPD approach for analyzing data, which is just one of several possible analytical approaches. It was used here over regression techniques because (a) some of the analytical relationships, either initially or at a later stage of synthesis, involved a small amount of data; and (b) no one method was assumed initially superior, so an unbiased parameterization of the differences between the methods was needed.

Traditional regression techniques are a common alternative to UPD statistics, but they can produce exaggerated parameters (e.g., slopes), and the data at the end points can have undue influence (or bias) on the regression when the dynamic range or population size of the variables is limited. The latter is particularly important for optical observations, because they are usually the most challenging areas for data collection, that is, they frequently represent overcast conditions, Case-2 waters, etc. At the final summary stage of the analysis (Table 7d), data density is potentially very good (a maximum of 95 samples can be considered for each intersection if the data are taken as one group), and the

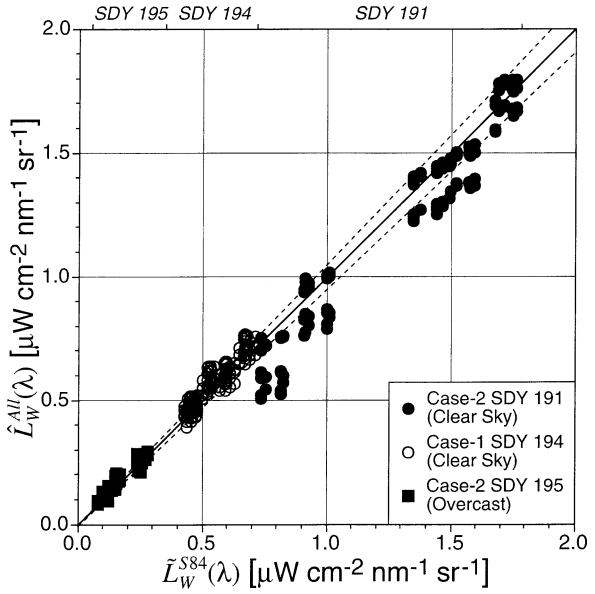

FIG. 8. The intracomparison of all of the above-water estimates of water-leaving radiance, $\hat{L}_W^{All}(\lambda)$, and the in-water estimates from the S84 method, $\tilde{L}_W^{S84}(\lambda)$, as a function of water type. The data falls neatly into the three sampling days as shown along the top of the graphic.

dynamic range is large (data samples are from clear and overcast sky, Case-1 and Case-2 waters, calm and roughened sea surface, etc.). Under these conditions, the limitations of regression analysis are reduced.

Regardless of the problems with least squares analyses, they are a ubiquitous tool in data analysis, so the method comparisons are re-evaluated using one such technique. Figure 8 presents the relationship between $\hat{L}_W^{All}(\lambda)$ versus $\tilde{L}_W^{S84}(\lambda)$, that is, all of the above-water methods regressed against the S84 (WP) in-water method. The large differences frequently associated with Case-2 conditions are clearly evident, as are the instances of small differences and the spectral properties of the differences. The level of agreement, as determined by the slope of the reduced major axis linear regression line (Ricker 1973; Press and Teukolsky 1992), m, and the coefficient of determination, R^2, is very good with a difference of approximately 6.0% ($m = 0.940$, $R^2 = 0.980$, and $N = 76$).

The Fig. 8 regression results are a little better than was obtained in Table 7d, for which the overall average difference for the above-water methods with respect to S84 was 7.7%. The difference between the two approaches is small and is probably an artifact of how the data were grouped for the UPD analyses. In Table 7d, averages were determined for each day of sampling, and the days were grouped independently for the final analysis. In Fig. 8, the data are handled as one large group, so the largest population of data (Case-1 with clear sky) contributes the most influence on the regression procedure, although, this is mitigated somewhat by the reasonably good distribution of the data (the dynamic range, in terms of radiance values, is fairly large).

The more informative relationships come from the individual regressions of the above-water methods against the S84 (WP) method (Fig. 9). Estimates of the intercomparison differences from the regression parameters are:

(a) M80 11.5% ($m = 0.885$, $R^2 = 0.975$, and $N = 19$),
(b) C85 3.6% ($m = 0.964$, $R^2 = 0.993$, and $N = 19$),
(c) S95 0.3% ($m = 1.003$, $R^2 = 0.994$, and $N = 19$), and
(d) L98 11.7% ($m = 0.893$, $R^2 = 0.986$, and $N = 19$).

The methods fall into two distinct groups: S95 and C85, and L98 and M80. This pairing of the methods is the same as given in Tables 7d and 8d for the S84 method. In each case, the percentage of variance explained is above 97%. Furthermore, a best-to-worst ranking based on the regression results is S95, C85, L98, and M80, which is also the same ranking from Tables 7d and 8d (the latter are based on the range of expected values formed from the averages and standard deviations). Although the rankings from the regression analysis agree with the UPD analysis, the estimated uncertainties from the former are a little larger for S95 and C85, and a little smaller for M80 and L98.

The regressions of all the above-water methods versus the P94 and P97 (in-water) methods also produce distinct ranking groups that are the same as the paired rankings already discussed: S95 and C85 have similar regression parameters as do L98 and M80. The estimated uncertainties between the methods using the regression technique yield values for P94 and P97 that differ from the spectral approach by approximately 5%. A regression of all the above-water methods versus all the in-water methods yields an intercomparison uncertainty of approximately 6.2% with about 97% of the variance explained ($m = 0.938$ and $R^2 = 0.969$). The spectrally averaged UPD analysis produced an overall uncertainty of 9.1% (Table 7d).

6. Conclusions

This study used data from three different environmental conditions that covered much of the dynamic range of in situ optical measurements, but, nonetheless, it was based on a small dataset collected during three days of measurements in the near-coastal environment. One of the three days (SDY 194) was within the parameter range established by the NRSR Workshop; the other two were not, but they were typical of the kinds of environmental conditions that can be encountered during above- and in-water radiometric field campaigns. Three in-water methods for determining water-leaving radiances from profiling (S84) and fixed-depth (P94 and P97) sampling systems were combined with four above-water methods to quantify the performance of all the

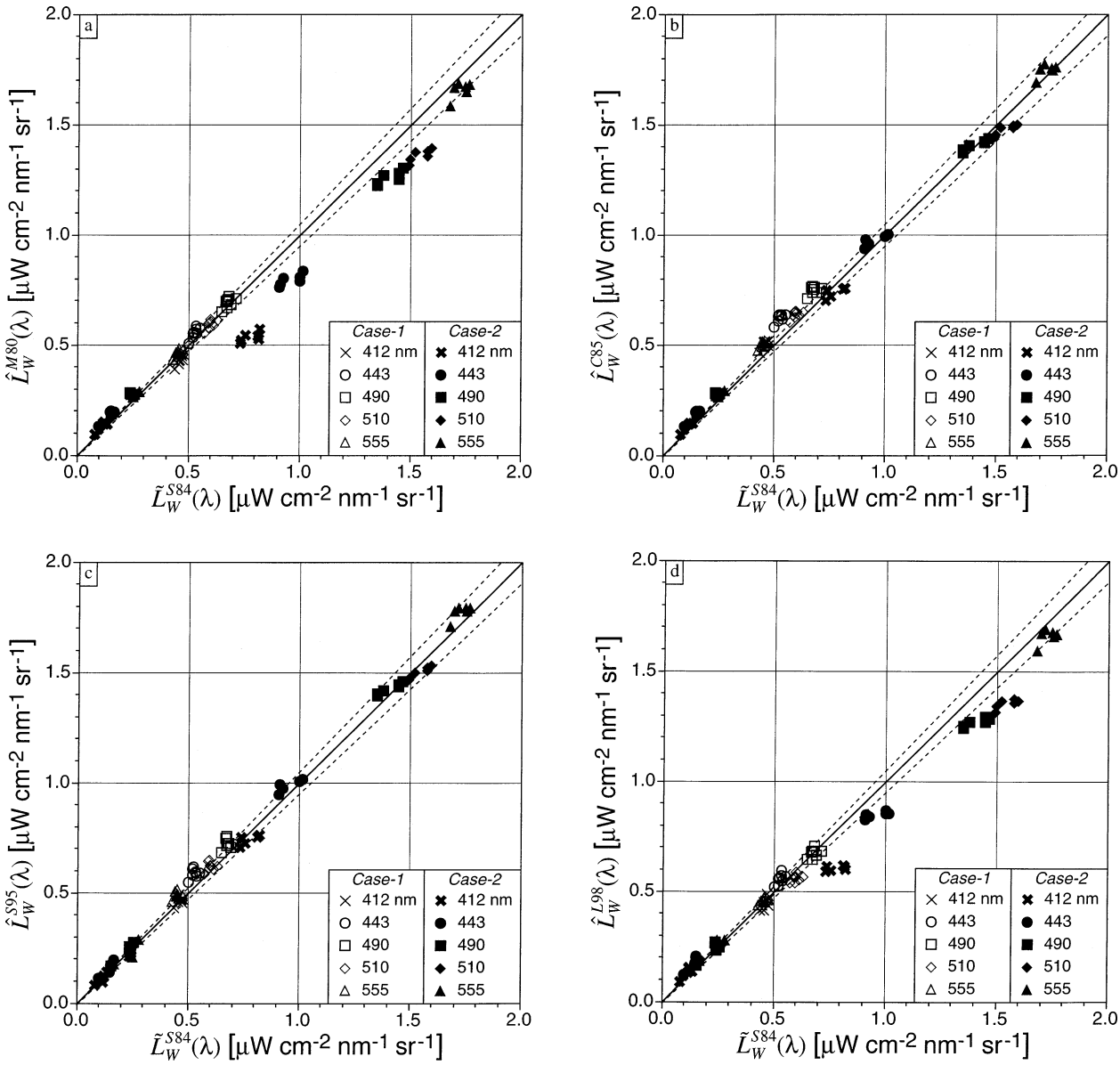

FIG. 9. The intercomparison of the individual above-water estimates of water-leaving radiance with the in-water estimates from the S84 method, $\tilde{L}_W^{S84}(\lambda)$, as a function of water type: (a) $\hat{L}_W^{M80}(\lambda)$, (b) $\hat{L}_W^{C85}(\lambda)$, (c) $\hat{L}_W^{S95}(\lambda)$, and (d) $\hat{L}_W^{L98}(\lambda)$. The dashed lines represent the ±5% limits with respect to the 1:1 line.

methods. The removal of glint contamination from the surface measurement distinguished the above-water methods from one another and included four correction schemes: near-infrared radiance ratio (M80), Fresnel reflectance plus residual reflection (C85), modified Fresnel reflectance (S95), and near-infrared irradiance ratio (L98).

The seven methods, three different days of environmental conditions, and five sampling platforms produced a large number of performance comparisons, which were separated according to UPD analyses based on spectral averages, band ratios, and discrete wavelengths. Although each method was usually found superior to the others at some stage in the performance evaluation process, the most suitable point for overall evaluation is at the intercomparison level summarized in Tables 6–9 and Figs. 8–9. Based on these summaries, some general capabilities concerning all the methods can be discerned.

1) In terms of the 5% calibration and validation objective, and the hoped for performance to within 3%, the spectral-average approach (Table 7d) produced larger average differences (and standard deviations) than the band-ratio approach (Table 8d), which were 9.1% (5.6%) and 3.7% (1.1%), respectively. Using

band ratios, the S84, P94, C85, and S95 methods produced ranges of expected differences (average plus and minus 1 standard deviation) within the 5% level, and frequently to within 3%.

2) The best results were not restricted to Case-1 or clear-sky conditions; water type was seen to be important, although other environmental parameters agreed well with the UPD levels (considered in more detail below). Consider, for example, the difficult circumstance of overcast conditions, which can be highly variable in terms of sky radiance distribution and relative (percent) variations in illumination conditions during a deployment interval. Because of the low signal levels, small absolute differences represent large relative discrepancies, but all the methods agreed very well for overcast conditions when using the data from the same instrument.
3) Above- and in-water methods not formulated for Case-2 conditions were capable of results in keeping with those achieved in Case-1 waters (e.g., Table 6). Agreement to within 5% was achieved with in-water methods in Case-1 waters for all three analytical approaches. Agreement within 5% was achieved with above-water methods in Case-2 waters for all analytical approaches, and was achieved in both water types for the band-ratio and discrete wavelength analyses (spectral averages were elevated due to large uncertainties in the blue domain).
4) For both above- and in-water methods, the largest uncertainties were usually associated with the blue part of the spectrum (412–443 nm), with the blue-green transition (490–510 nm) a local minimum, which was followed by a small increase at 555 nm (Table 9). The above-water methods that calculated the surface reflectance by assuming $\lambda_r = 0$ (M80 and L98) were spectrally dependent during Case-2, clear-sky conditions, with very large uncertainties at 412 nm (as much as 38%) and minimum uncertainties at 555 nm (less than 5%).

Note that all of the analytical approaches yielded average uncertainties across all three days and all methods below the 10% level, so for applications where this level of agreement is acceptable—for example, perhaps with large-scale bio-optical models, any of the methods are probably acceptable. It is also important to remember the regression analysis results confirm these overall conclusions (although there are small shifts in the magnitude of the uncertainties).

For the in-water methods alone, the specific details of the capabilities of the methods are as follows.

5) P94 and P97 grouped together, but S84 performed the best. Consequently, an in-water method making use of vertical profiles of the water column should be considered superior than those using sensors at a fixed depth, although good results were obtained for the latter during Case-1 conditions and for band-ratio analyses.
6) The best-to-worst ranking of the in-water methods (using the minimal range in average differences) did not depend on the analytical approach (S84, P94, and P97), but the ranking of the above-water methods did (S95, L98, C85, and M80 for the spectrally averaged approach; and C85, S95, M80, and L98 for the band-ratio approach).
7) The in-water spectral averages intracompared best during Case-1 conditions and worst during Case-2 conditions (Table 7c), which is consistent with the higher variability associated with the latter; however, the opposite result was seen with the band-ratio analysis (Table 8c).

Before considering the above-water methods separately, it is important to remember proper data filtering to remove glint spikes is an essential part of above-water methods that permit it (the C85 method does not). Although many schemes were considered in this study (section 3c), the adopted filter retained only the lowest 5% of the data, based on the reddest (780-nm) band. Similarly, data averaging was shown to needlessly and significantly degrade the quality of the above-water data because it artificially elevated the $L_T(\lambda)$ values by contaminating them with glint. Subsampling did not degrade the above-water data as significantly as averaging, but it showed that above-water sampling rates should be equal to, or greater than, 1 Hz (Fig. 7). The conclusion to be derived here is the glint field must be adequately discretized, so it can be removed by filtering. The other conclusions for the above-water methods alone are as follows.

8) S95 and C85 grouped together and outperformed L98 and M80, which also grouped together, with S95 performing the best overall (well demonstrated in the Table 9 results and confirmed by the regression analyses in section 5).
9) Intracomparisons of above-water methods during Case-2 conditions yielded both the best and worst agreement in terms of spectral averages (Table 7c) and band ratios (Table 8c), but this could have been due more to surface roughness and sky conditions than water type.

Relative (signed) differences were not the primary statistical tool in this study, but the Fig. 9 intercomparisons between the S85 and the above-water methods showed L98 and M80 underestimated $\hat{L}_w(\lambda)$ during clear-sky, Case-2 conditions; C85 and S95 overestimated $\hat{L}_w(\lambda)$ during clear-sky, Case-1 conditions; and M80 and C85 overestimated $\hat{L}_w(\lambda)$ during overcast, Case-2 conditions. These performance biases are largely in keeping with the design characteristics of the above-water methods (Table 3).

With respect to synthesizing the performance of the above- and in-water methods in different water types, it is important to remember the explicit caution about using the M80, L98, and P97 methods in Case-2 waters.

In terms of the C85 method and its published use within different water types, that is, the value of the $R_{rs}(440)/R_{rs}(550)$ ratio, for SDY 191, 194, and 195, the ratio has values of 0.49, 1.22, and 0.69, respectively. These ratios indicate the method can be used uncertainly (almost cautiously), confidently, and cautiously, respectively. For all of these methods, however, there is the counterbalancing evidence that they all performed well in Case-2 conditions in many instances, and in some cases, were comparable to the best methods (particularly in the case of the band-ratio results).

The efforts to categorize the method performance as a function of water type deserve extra comment. First of all, a primary discriminator of Case-2 suitability is whether or not the $\hat{L}_w(\lambda_r) = 0$ assumption is made. It is important to remember this assumption is not restricted to Case-1 conditions as long as the sediment concentration is not significant, that is, Case-2 waters not characterized by a heavy sediment load (as is usually the case in the Adriatic Sea). Second, the scheme used for classifying water types (Loisel and Morel 1998) indicated each day was close to the boundary between Case-1 and Case-2 waters. Third, the data set considered here was sufficiently small that other variables might explain differences in the methods besides water type. For example, the S95 method is not sensitive to water type, but was formulated for a flat sea, and clear sky. The SeaSAS and DalSAS results (Table 6) agree well on SDY 191 (Case-2, flat sea surface, and clear sky), they do not agree well on SDY 194 (Case-1, rough sea surface, and clear sky), and they do not agree on SDY 195 (Case-2, calm sea surface, and overcast and more variable sky). The performance of the method does correlate with water type, but it also correlates with surface and sky conditions.

Taking the water-type classification issues into account, some additional capabilities about the methods emerge.

10) M80 and L98 appeared less sensitive to surface roughness (they produced the best agreement with the in-water methods on the roughest day, SDY 194) and always performed well when $\hat{L}_w(\lambda_r) = 0$. Uncertainties in S95 and C85 introduced by surface roughness were smaller than the uncertainties in M80 and L98 introduced by $\hat{L}_w(\lambda_r) > 0$ (Case-2 water).
11) S95 and C85 were sensitive to surface roughness, and C85 to some extent on water type. Both methods performed well in Case-2 conditions, but in the case of a rough sea surface, both methods tended to overestimate $\hat{L}_w(\lambda)$ values (C85 up to 14% and S95 up to 10% in comparison to S84).
12) For the special case of a single method applied to two instruments measuring simultaneously, the above-water techniques showed a sensitivity as to whether or not the instruments were pointed in the same (best agreement) or opposite (worst agreement) directions, while still satisfying the sampling protocols; no methodological dependencies were seen with the use of the same in-water method on two data streams.

For the latter, it is important to remember agreement close to 3% was achieved for both above- and in-water measurements. For in-water measurements from two instruments (WiSPER and miniNESS) and one method (S84), during Case-1 conditions (SDY 194), the uncertainty between the two was to within 3.4%, which is in keeping with the Hooker and Maritorena (2000) Case-1 (open ocean) results. During Case-2 conditions (SDY 191 and 195), however, the uncertainty increased (on average) by about a factor of 2 to approximately 7.8%, and the overall uncertainty (across all three days) was slightly above 5% (at the 6.3% level). The latter was sufficiently close to 5% that there is reason to believe additional care in the acquisition procedures (e.g., precision depth sensors and faster sampling rates to better resolve vertical structure and surface effects) would produce data products within the 5% objective.

For above-water measurements from two instruments (SeaSAS and DalSAS) and one method (S95), the difference between the two viewing possibilities associated with pointing an above-water radiometer $\pm 90^\circ$ with respect to the sun introduced (on average) an additional 3%–7% of variability. It is probably caused by surface waves (and wind), inhomogeneities in the sky radiance field, and geometrical aspects (i.e., a dependence on the direction of the ambient swell with respect to the instruments, the sun, and the wind): one instrument is viewing a reflection field that is brightened and roughened by the wave crests, and the other a reflection field that is darkened and smoothed by the wave troughs. This poses many practical problems with the proper deployment of an above-water system on a moving vessel or a fixed platform because there are always preferred pointing directions due to obstructions, platform orientation with respect to the sun and waves, etc.

Acknowledgments. SeaBOARR-98 could not have been executed at the high level that was achieved without the competent contributions of the AAOT crew: Armando and Daniele Penzo, and Narciso and Gianni Zennaro. The logistics were substantially more involved than the usual CoASTS field campaigns, so the enthusiastic assistance from the CNR scientific staff led by Luigi Alberotanza was essential. In particular, Perluigi Cova was responsible for the CTD profiles as well as the meteorological data collection, and Sandro Vianello was responsible for water filtration. Acknowledgments are also due to the JRC scientists: Dirk van der Linde for the support provided in preparing the optical devices for deployment and the TSM analyses, John Doyle for miniNESS deployment assistance, Jean-François Berthon for providing the AC-9 processed data, Cristina Targa for the HPLC analyses, and Stefania Grossi for

the dissolved and particulate matter absorption analyses. The JRC and CNR participation in the experiment was mainly supported by the European Commission through Contracts ENV4-CT96-0307 and MAS3-CT97-0087. The miniNESS, SeaSAS, DalSAS, and DalBOSS data were all acquired and recorded using software developed by Jim Brown (University of Miami) and the SeaWiFS Project. The SeaWiFS Project (Charles McClain) also provided additional funding, directly or indirectly, to most of the participants, which was critical in bringing all of the needed elements together as scheduled. The final preparation of the manuscript benefitted from the editorial and logistical assistance of Elaine Firestone.

APPENDIX A

Glossary

AAOT *Acqua Alta* Oceanographic Tower
C85 The above-water method for determining water-leaving radiances based on Carder and Steward (1985), and as further explained in Lee et al. (1996)
DalBOSS Dalhousie Buoyant Optical Surface Sensor (abbreviated DB)
DalSAS Dalhousie SeaWiFS Aircraft Simulator (abbreviated DS)
L98 The above-water method for determining water-leaving radiances based on Lazin (1998)
M80 The above-water method for determining water-leaving radiances based on Morel (1980)
miniNESS miniature NASA Environmental Sampling System (abbreviated MN)
NRSR Normalized Remote Sensing Reflectance (workshop held 11–12 December 1997)
P94 The in-water (surface buoy) method for determining water-leaving radiances as implemented in ProSoft in 1994
P97 The in-water (surface buoy) method for determining water-leaving radiances as implemented in ProSoft in 1997
S84 The in-water (vertical profile) method for determining water-leaving radiances based on Smith and Baker (1984)
S95 The above-water method for determining water-leaving radiances based on Mueller and Austin (1995), and as revised in Mueller et al. 2000
SDY Sequential Day of the Year
SeaBOARR SeaWiFS Bio-Optical Algorithm Round-Robin
SeaSAS SeaWiFS Surface Acquisition System (abbreviated SS)
SeaWiFS Sea-viewing Wide Field-of-view Sensor
SQM SeaWiFS Quality Monitor
SQM-II The second generation SeaWiFS Quality Monitor
UPD Unbiased Percent Difference
WiSPER Wire-Stabilized Profiling Environmental Radiometer

APPENDIX B

Primary Symbols

$E_d(\lambda)$ The spectral downward irradiance
$E_d(0^+, \lambda)$ The total solar irradiance just above the sea surface
$E_i(0^+, \lambda)$ The diffuse solar irradiance just above the sea surface
$E_u(\lambda)$ The spectral upwelled irradiance
$K(\lambda)$ The diffuse attenuation coefficient
$K_{L_u}(\lambda)$ The diffuse attenuation coefficient for upwelling radiance
$L_i(0^+, \lambda)$ The sky radiance reaching the sea surface
$L_p(0^+, \lambda)$ The (gray) plaque radiance
$L_T(0^+, \lambda)$ The total radiance right above the sea surface
$L_u(\lambda)$ The spectral upwelled radiance
$L_W(\lambda)$ Spectral water-leaving radiance
$L_W(\lambda_{k/l})$ The $L_W(\lambda_k)/L_W(\lambda_l)$ ratio
$\hat{L}_W(\lambda)$ Spectral water-leaving radiance determined from an above-water measurement
$\tilde{L}_W(\lambda)$ Spectral water-leaving radiance determined from an in-water measurement
θ The solar zenith angle
ϑ The above-water instrument nadir and zenith angles during data collection ($\vartheta = 40°$)
ϑ' The above-water instrument zenith angle measured from nadir ($\vartheta' = 140°$)
λ_r A wavelength or channel in the near-infrared part of the spectrum
ϕ The solar azimuth angle
ϕ' The above-water instrument azimuth angle during data collection ($\phi' = \phi \pm 90°$)
$\Phi_B^A(\lambda_{k/l})$ The UPD between band ratios of water-leaving radiances for wavelengths k and l (12)
$\rho(\lambda)$ The Fresnel reflectance coefficient
ρ' The effective (and spectrally constant) surface reflectance
$\psi_B^A(\lambda)$ The unbiased percent difference (UPD) between two data products X^A and X^B (9)
$\overline{\psi}_B^A(\lambda)$ The average UPD values over a particular set of data (10)
$\Psi_B^A(\lambda_{1-5})$ The spectrally averaged UPD (11)

REFERENCES

Aiken, J., and Coauthors, 1998: AMT-5 cruise report. S. B. Hooker and E. R. Firestone, Eds., NASA Tech. Memo. 1998–206892,

Vol. 2, 113 pp. [Available from Center for Aerospace Information, 7121 Standard Dr., Hanover, MD, 21076-1320.]

Austin, R. W., 1974: The remote sensing of spectral radiance from below the ocean surface. *Optical Aspects of Oceanography,* N. G. Jerlov and E. S. Nielsen, Eds., Academic Press, 317–344.

——, 1980: Gulf of Mexico, ocean–color surface–truth measurements. *Bound.-Layer Meteor.,* **18,** 269–285.

——, and T. J. Petzold, 1981: The determination of diffuse attenuation coefficient of sea water using the Coastal Zone Color Scanner. *Oceanography from Space,* J. F. R. Gower, Ed., Plenum Press, 239–256.

Bukata, R. P., J. H. Jerome, and J. E. Bruton, 1988: Particulate concentrations in Lake St. Clair as recorded by shipborne multispectral optical monitoring system. *Remote Sens. Environ.,* **25,** 201–229.

——, ——, K. Y. Kondrattyev, and D. V. Pozdnyakov, 1995: *Optical Properties and Remote Sensing of Inland and Coastal Waters.* CRC Press, 362 pp.

Carder, K. L., and R. G. Steward, 1985: A remote sensing reflectance model of a red tide dinoflagellate off West Florida. *Limnol. Oceanogr.,* **30,** 286–298.

Ferrari, G. M., M. D. Dowell, S. Grossi, and C. Targa, 1996: Relationship between the optical properties of chromophoric dissolved organic matter and total concentration of dissolved organic carbon in the southern Baltic Sea region. *Mar. Chem.,* **55,** 299–316.

Fougnie, B., P.-Y. Deschamp, and R. Frouin, 1999: Vicarious calibration of the POLDER ocean color spectral bands using in situ measurements. *Trans. IEEE Trans. Geosci. Remote Sens.,* **37,** 1567–1574.

Gordon, H. R., 1981: A preliminary assessment of the Nimbus-7 CZCS atmospheric correction algorithm in a horizontally inhomogeneous atmosphere. *Oceanography from Space,* J. F. R. Gower, Ed., Plenum Press, 257–266.

——, and M. Wang, 1994: Retrieval of water-leaving radiances and aerosol optical thickness over the oceans with SeaWiFS: A preliminary algorithm. *Appl. Opt.,* **33,** 443–452.

Hooker, S. B., 2000: Stability monitoring of field radiometers using portable sources. Ocean Optics Protocols for Satellite Ocean Color Sensor Validation, Rev. 2, G. S. Fargion and J. L. Mueller, Eds., NASA Tech. Memo. 2000–209966. 57–64. [Available from NASA Center for Aerospace Information, 7121 Standard Dr., Hanover, MD 21076-1320.]

——, and W. E. Esaias, 1993: An overview of the SeaWiFS project. *Eos, Trans. Amer. Geophys. Union,* **74,** 241–246.

——, and J. Aiken, 1998: Calibration evaluation and radiometric testing of field radiometers with the SeaWiFS Quality Monitor (SQM). *J. Atmos. Oceanic Technol.,* **15,** 995–1007.

——, and G. Lazin, 2000: The SeaBOARR-99 field campaign. S. B. Hooker and E. R. Firestone, Eds., NASA Tech. Memo. 2000–206892, Vol. 8, 46 pp. [Available from NASA Center for Aerospace Information, 7121 Standard Dr., Hanover, MD 21076-1320.]

——, and S. Maritorena, 2000: An evaluation of oceanographic radiometers and deployment methodologies. *J. Atmos. Oceanic Technol.,* **17,** 811–830.

——, and C. R. McClain, 2000: The calibration and validation of SeaWiFS data. *Progress in Oceanography,* Vol. 45, Pergamon, 427–465.

——, W. E. Esaias, G. C. Feldman, W. W. Gregg, and C. R. McClain, 1992: An overview of SeaWiFS and ocean color. S. B. Hooker and E. R. Firestone, Eds., NASA Tech. Memo. 104566, Vol. 1, 24 pp. [Available from NASA Center for Aerospace Information, 7121 Standard Dr., Hanover, MD 21076-1320.]

——, ——, and L. A. Rexrode, 1993a: Proceedings of the first SeaWiFS science team meeting. S. B. Hooker and E. R. Firestone, Eds., NASA Tech. Memo. 104566, Vol. 8, 61 pp. [Available from NASA Center for Aerospace Information, 7121 Standard Dr., Hanover, MD 21076-1320.]

——, C. R. McClain, and A. Holmes, 1993b: Ocean color imaging: CZCS to SeaWiFS. *Mar. Tech. Soc. J.,* **27,** 3–15.

——, ——, J. K. Firestone, T. L. Westphal, E.-n., Yeh, and Y. Ge, 1994: The SeaWiFS Bio-Optical Archive and Storage System (SeaBASS). Part 1. S. B. Hooker and E. R. Firestone, Eds., NASA Tech. Memo. 104566, Vol. 20, 40 pp. [Available from NASA Center for Aerospace Information, 7121 Standard Dr., Hanover, MD 21076-1320.]

——, G. Zibordi, G. Lazin, and S. McLean, 1999: The SeaBOARR-98 field campaign. S. B. Hooker and E. R. Firestone, Eds., NASA Tech. Memo. 1999–206892, Vol. 3, 40 pp. [Available from NASA Center for Aerospace Information, 7121 Standard Dr., Hanover, MD 21076-1320.]

——, S. Maritorena, J.-F. Berthon, D. D'Alimonte, G. Zibordi, S. McLean, and J. Sildam, 2001: Results of the second SeaWiFS Data Analysis Round-Robin, March 2000 (DARR-00). S. B. Hooker and E. R. Firestone, Eds., NASA Tech. Memo. 2001–206892, Vol. 15, 71 pp. [Available from NASA Center for Aerospace Information, 7121 Standard Dr., Hanover, MD 21076-1320.]

——, S. McLean, J. Sherman, M. Small, G. Zibordi, and J. Brown, 2002: The Seventh SeaWiFS Intercalibration Round-Robin Experiment (SIRREX-7), March 1999. S. B. Hooker and E. R. Firestone, Eds., NASA Tech. Memo. 2002–206892, Vol. 17, 69 pp. [Available from NASA Center for Aerospace Information, 7121 Standard Dr., Hanover, MD 21076-1320.]

Jeffrey, S. W., R. F. C. Mantoura, and S. W. Wright, Eds., 1997: *Phytoplankton Pigments in Oceanography: Guidelines to Modern Methods.* UNESCO Publishing, 661 pp.

Johnson, B. C., S. S. Bruce, E. A. Early, J. M. Houston, T. R. O'Brian, A. Thompson, S. B. Hooker, and J. L. Mueller, 1996: The Fourth SeaWiFS Intercalibration Round-Robin Experiment (SIRREX-4), May 1995. S. B. Hooker and E. R. Firestone, Eds., NASA Tech. Memo. 104566, Vol. 37, 65 pp. [Available from NASA Center for Aerospace Information, 7121 Standard Dr., Hanover, MD 21076-1320.]

——, P. S. Shaw, S. B. Hooker, and D. Lynch, 1998: Radiometric and engineering performance of the SeaWiFS Quality Monitor (SQM): A portable light source for field radiometers. *J. Atmos. Oceanic Technol.,* **15,** 1008–1022.

Joint Global Ocean Flux Study, 1994: Protocols for the Joint Global Ocean Flux Study core measurements. Intergovernmental Oceanographic Commission, Scientific Committee on Oceanic Research. *UNESCO,* **29,** 91–96.

Lazin, G., 1998: Correction methods for low-altitude remote sensing of ocean color. M.S. thesis, Dept. of Oceanography, Dalhousie University, 98 pp.

Lee, Z. P., K. L. Carder, R. G. Steward, T. G. Peacock, C. O. Davis, and J. L. Mueller, 1996: Remote sensing reflectance and inherent optical properties of oceanic waters derived from above-water measurements. *Proc. SPIE, Ocean Optics XIII,* Vol. 2963, SPIE, 160–166.

Loisel, H., and A. Morel, 1998: Light scattering and chlorophyll concentration in case 1 waters: A reexamination. *Limnol. Oceanogr.,* **43,** 847–858.

McLean, S., S. Feener, J. Scrutton, M. Small, S. Hooker, and M. Lewis, 1998: SQM-II: A commercial portable light source for field radiometer quality assurance. *Proc. Ocean Optics XIV,* Office of Naval Research, CD-ROM.

Mobley, C. D., 1999: Estimation of the remote-sensing reflectance from above-surface measurements. *Appl. Opt.,* **38,** 7442–7455.

Morel, A., 1980: In-water and remote measurements of ocean color. *Bound.-Layer Meteor.,* **18,** 177–201.

——, 1988: Optical modeling of the upper ocean in relation to its biogenous matter content (Case I waters). *J. Geophys. Res.,* **93,** 10749–10768.

Mueller, J. L., 2000: In-water radiometric profile measurements and data analysis protocols. Ocean Optics Protocols for Satellite Ocean Color Sensor Validation, Rev. 2, G. S. Fargion and J. L. Mueller, Eds., NASA Tech. Memo. 2000–209966, 87-97. [Avail-

able from NASA Center for Aerospace Information, 7121 Standard Dr., Hanover, MD 21076-1320.]

——, and R. W. Austin, 1992: Ocean optics protocols for SeaWiFS validation. S. B. Hooker and E. R. Firestone, Eds., NASA Tech. Memo. 104566, Vol. 5, 43 pp. [Available from NASA Center for Aerospace Information, 7121 Standard Dr., Hanover, MD 21076-1320.]

——, and ——, 1995: Ocean optics protocols for SeaWiFS validation. Rev. 1, S. B. Hooker and E. R. Firestone, Eds., NASA Tech. Memo. 104566, Vol. 25, 66 pp. [Available from NASA Center for Aerospace Information, 7121 Standard Dr., Hanover, MD 21076-1320.]

——, B. C. Johnson, C. L. Cromer, S. B. Hooker, J. T. McLean, and S. F. Biggar, 1996: The third SeaWiFS Intercalibration Round-Robin Experiment (SIRREX-3), 19–30 September 1994. S. B. Hooker and E. R. Firestone, Eds., NASA Tech. Memo. 104566, Vol. 34, 78 pp. [Available from NASA Center for Aerospace Information, 7121 Standard Dr., Hanover, MD 21076-1320.]

——, and Coauthors, 2000: Above-water radiance and remote sensing reflectance measurement and analysis protocols. Ocean Optics Protocols for Satellite Ocean Color Sensor Validation, Rev. 2, G. S. Fargion and J. L. Mueller, Eds., NASA Tech. Memo. 2000–209966, 98-107. [Available from NASA Center for Aerospace Information, 7121 Standard Dr., Hanover, MD 21076-1320.]

O'Reilly, J. R., S. Maritorena, B. G. Mitchell, D. A. Siegel, K. L. Carder, S. A. Garver, M. Kahru, and C. McClain, 1998: Ocean color chlorophyll algorithms for SeaWiFS. *J. Geophys. Res.,* **103,** 24 937–24 953.

Pinkerton, M. H., C. C. Trees, J. Aiken, A. J. Bale, G. F. Moore, R. G. Barlow, and D. G. Cummings, 1999: Retrieval of near-surface bio-optical properties of the Arabian Sea from remotely sensed ocean colour data. *Deep-Sea Res. Part II,* **46,** 549–569.

Press, W. H., and S. A. Teukolsky, 1992: Fitting straight line data with errors in both coordinates. *Comput. Phys.*, **6,** 274–276.

Ricker, W. E., 1973: Linear regressions in fishery research. *J. Fish. Res. Board Can.*, **30,** 409–434.

Siegel, D. A., and Coauthors, 1995: Results of the SeaWiFS Data Analysis Round-Robin (DARR-94), July 1994. S. B. Hooker and E. R. Firestone, Eds., NASA Tech. Memo. 104566, Vol. 26, 58 pp. [Available from NASA Center for Aerospace Information, 7121 Standard Dr., Hanover, MD 21076-1320.]

Smith, R. C., and K. S. Baker, 1984: The analysis of ocean optical data. *Ocean Optics VII,* M. Blizard, Ed., Proceedings of SPIE—The International Society for Optical Engineering, Vol. 478, SPIE, 119–126.

——, and ——, 1986: Analysis of ocean optical data II. *Ocean Optics VIII,* P. N. Slater, Ed., Proceedings of SPIE—The International Society for Optical Engineering, Vol. 637, SPIE, 95–107.

Strickland, J. D. H., and T. R. Parsons, 1972: *A Practical Handbook of Sea Water Analysis.* Fisheries Research Board of Canada, 310 pp.

Tassan, S., and M. Ferrari, 1995: An alternative approach to absorption measurements of aquatic particles retained on filters. *Limnol. Oceanogr.,* **40,** 1358–1368.

Toole, D. A., D. A. Siegel, D. W. Menzies, M. J. Neumann, and R. C. Smith, 2000: Remote sensing reflectance determinations in the coastal ocean environment—Impact of instrumental characteristics and environmental variability. *Appl. Opt.,* **39,** 456–469.

Zibordi, G., and M. Ferrari, 1995: Instrument self-shading in underwater optical measurements: Experimental data. *Appl. Opt.,* **34,** 2750–2754.

——, J. P. Doyle, and S. B. Hooker, 1999: Offshore tower shading effects on in-water optical measurements. *J. Atmos. Oceanic Technol.,* **16,** 1767–1779.